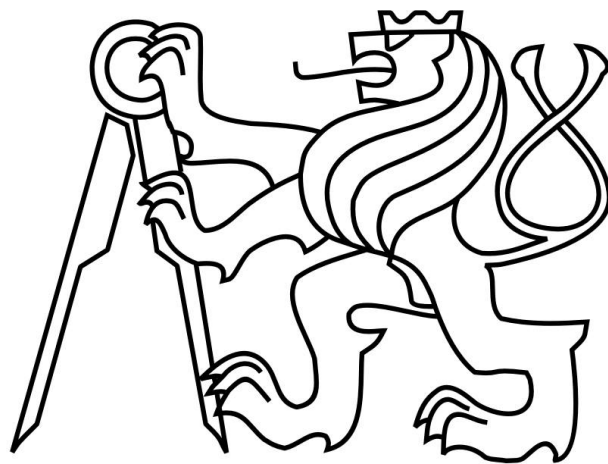# CZECH TECHNICAL UNIVERSITY IN PRAGUE

12105 Department of Mechanics, Biomechanics and Mechatronics

MASTER'S THESIS

Fatigue Analysis of a Blade of the H80 Engine Impeller

Jitka Pfeiferová   **2015/2016**

Abstract

This master thesis deals with fatigue life assessment of the H80 engine impeller alternative design. 4 different methods of fatigue life calculation are presented and consequently used to predict the life of the impeller. Furthermore, the thermal and structural FEM analysis of the impeller was carried out in order to obtain the stress-strain state of the component for the fatigue life assessment.

Keywords

Declaration

This thesis is a presentation of my original research work. Wherever contributions of others are involved, every effort is made to indicate this clearly, with due reference to the literature, and acknowledgement of collaborative research and discussions. The work was done under the guidance of Ing. Jan Papuga Ph.D., at the Czech Technical University, Prague.

Date:.. Signature:..

Acknowledgement

Contents

List of Figures

List of Tables

Nomenclature

α, β, γ	The Prandtl density
$\bar{\sigma}_{\max}$	Maximum stress tensor from the load cycle
$\bar{\sigma}_{\min}$	Minimum stress tensor from the load cycle
$\Delta\epsilon_{real}$	Elastoplastic strain range in the load cycle
$\Delta\sigma_{elastic}$	Elastic stress range in the load cycle
$\Delta\sigma_{real}$	Elastoplastic stress range in the load cycle
$\Delta\sigma_x, \Delta\sigma_y, \Delta\sigma_z$	Normal stress range in the load cycle in X, Y and Z direction
$\Delta\tau_{xy}, \Delta\tau_{yz}, \Delta\tau_{xz}$	Shear stress range in the load cycle in XY, YZ and XZ direction
$\epsilon_{a,e}$	Elastic strain amplitude
$\epsilon_{a,p}$	Plastic strain amplitude
$\epsilon_{alt,e}$	Elastic alternating strain
$\epsilon_{alt,p}$	Plastic alternating strain
ϵ_{alt}	Alternating strain
ϵ_a	Strain amplitude
$\epsilon_{elastic}$	Pseudo elastic strain
ϵ'_f	Fatigue ductility exponent
$\mathcal{F}_r$	The play operator
ω	Rotational velocity
ρ	Density
$\sigma_1, \sigma_2, \sigma_3$	1st, 2nd and 3rd principal stress
σ_α	The play operator for total strain determination
$\sigma_{\gamma j}$	The play operator for damage determination
$\sigma_{\max, FE}$	Maximum elastic stress in the load cycle

$\sigma_{\max_x}, \sigma_{\max_y}, \sigma_{\max_z}$	Maximum normal stress from the load cycle in X, Y and Z direction
$\sigma_{\min_x}, \sigma_{\min_y}, \sigma_{\min_z}$	Minimum normal stress from the load cycle in X, Y and Z direction
$\sigma_{a,FE}$	Elastic stress amplitude
σ_{alt}	Alternating stress
σ_a	Stress amplitude
$\sigma_{e,svM}$	elastic signed Von Mises stress
$\sigma_{elastic}$	Pseudo elastic stress
σ'_f	Fatigue strength exponent
$\sigma_{m,FE}$	Elastic mean stress
σ_{max}	Maximum stress experienced during the load cycle
σ_{min}	Minimum stress experienced during the load cycle
σ_m	Mean stress
σ_{Neuber}	Neuber parameter
σ_{real}	Elastoplastic stress
σ_{SWT}	Smith-Watson Topper parameter
$\tau_{\max_{xy}}, \tau_{\max_{yz}}, \tau_{\max_{xz}}$	Maximum shear stress from the load cycle in XY, YZ and XZ direction
$\tau_{\min_{xy}}, \tau_{\min_{yz}}, \tau_{\min_{xz}}$	Minimum shear stress from the load cycle in XY, YZ and XZ direction
b	Fatigue strength coefficient
c	Fatigue ductility coefficient
c_p	Specific heat at a constant pressure
D	Damage
D_{accum}	Cumulative damage

d_f	Cycle damage
E	Young's modulus
E_{cyc}	Cyclic Young's modulus
K	Hardening coefficient
k	Thermal conductivity coefficient
K'	Cyclic hardening coefficient
M	Interpolation coefficient
N	Number of cycles to crack initiation (Fatigue life)
n	Hardening exponent
n'	Cyclic hardening exponent
n_r	Length of the vector with Prandtl densities
q	Heat generation rate per unit volume
R	Load ratio
r	Fictive yield stress
T	Temperature
t	time
$T_{\max}$	Temperature at maximum peak of the load cycle
$T_{\min}$	Temperature at minimum peak of the load cycle
v	Input function of the play operator
w	Output function of the play operator
x	Interpolation exponent

1 Introduction

Nowadays, components of aircraft engines are subjected to cyclic loading caused by their operation since they are repeatedly switched on and turned off. Frequently, due the the high loads, high plastic strains occur in these components that usually result in low cycle fatigue. Hence, the components can withstand only limited time in service before a failure occurs. Fatigue can affect any component but it is usually the most significant for rotating parts such as turbines and compressors.

There are different approaches developed that describe how to assess low cycle fatigue and predict the life of the component. However, each of this approaches have its drawbacks. 4 different methods of low cycle fatigue assessment are presented in this thesis. Consequently, these 4 methods are applied to estimate a fatigue life of the impeller alternative design in H80 engine produced by GE BGA Turboprops.

The aim of this thesis is to perform the low cycle fatigue calculation of H80 engine impeller alternative design by use of these 4 methods: historical GEAC method, SWT method, Landgraf method and method proposed by Nagode and then assess the results. Attention is focused on the results comparison and interpretation as well as explanation of the possible differences.

To begin with, the FEM analysis is performed in order to obtain stress-strain state of the impeller. Then, based on the results from FEM, the SWT and Landgraf method is used to calculate fatigue life in each node of the FEM model. Afterwards, the most critical locations are chosen and fatigue life is estimated for them using the historical GEAC method and method proposed by Nagode. Finally, the results obtained from all the methods are compared.

2 Fatigue

Fatigue is weakening of the structure caused by applied cyclic loading. The damage appears after a certain number of load cycles at nominal stress level that is usually far below the static tensile strength of the material. This is one of the reasons why fatigue is one of the most frequent sources of failure of materials. Moreover, it affects all materials, without exception. The process until the structure fails due to the fatigue comprises 3 stages. That is: crack nucleation, crack propagation and rapid failure. Firstly, the damage occurs on the microscopic level, then it propagates until a crack on macroscopic level is reached. Subsequently, the macroscopic crack grows further until it reaches a critical size. At this point the structure cannot sustain the load any more and it fails. The number of load cycles that the structure can sustain until the crack occurs is called fatigue life N. The variable that influences the fatigue life the most is a stress amplitude of the load cycle that is defined as follows:

$$\sigma_a = \frac{\sigma_{max} - \sigma_{min}}{2} \tag{2.1}$$

where σ_{max} and σ_{min} are maximum and minimum stresses experienced during the load cycle, respectively. However, a mean stress defined as:

$$\sigma_m = \frac{\sigma_{max} + \sigma_{min}}{2} \tag{2.2}$$

has also significant influence on the fatigue life and should be taken into consideration.

Usually, our load history is not defined by only one load cycle but it consists of varying loads. In order to deal with this fact, a rainflow-counting algorithm is commonly used. This method transforms a spectrum of varying loads into set of simple load cycles. Each of this cycle is defined by its amplitude σ_a and mean stress σ_m. The advantage of this method is that it can be used as an input to Miner's Rule. The Miner's rule is a cumulative damage model that combines individual load cycle extracted from rainflow counting and determines number of equivalent load cycles until failure.

The procedure of fatigue life evaluation can be summarized into general steps that are usually common for all the fatigue evaluation methods. These steps are:

1. Determination of stress-strain response to our load history, usually with FEA

2. Conversion of multiaxial stress state into uniaxial stress state

3. Elastoplastic correction of the stress and strain histories if the linear FEA in step 1 was used

4. Rainflow counting to convert a random load history to a sequence of separate load cycles

5. A damage parameter calculation for each load cycle extracted from the rainflow counting

6. A fatigue life determination for each cycle extracted from the rainflow counting using material curves

7. A number of equivalent load cycles to failure estimation based on a cumulative damage model

Fatigue is commonly divided into 2 categories: low-cycle fatigue(LCF) and high-cycle fatigue(HCF). This division is based on fatigue life N when the boundary between them is not exact but it is usually of the order of 100 000 load cycles. HCF is usually represented by low enough stresses so that only elastic strains occur, whereas during LCF inelastic stresses are usually involved as well.

2.1   High-cycle fatigue

As already mentioned above, HCF occurs when fatigue life N exceeds certain number of cycles, it is usually approximately 10^5 or more. The loads are usually not that high, thus the deformation is within an elastic range. However, the plastic deformation can appear at the crack tip. In case of HCF, we use the Stress Life Method that uses the Stress-Life curve for fatigue evaluation. It is curve with a stress amplitude on y-axis against the fatigue life N on the x-axis. This curve is utilized to determine an allowable stress amplitude for an assumed service life of the component.

2.2   Low-cycle fatigue

Low-cycle fatigue is a result of repeated plastic deformation in the locations of the component with stress concentrations. It is typical for the components that work under high operation load. The fatigue life is usually determined using strain-life approach when the Manson-Coffin equation is utilized. It is a relation between the plastic strain amplitude and the number of load cycles to failure N described by the

following formula:

$$\epsilon_{a,p} = \epsilon'_f (2N)^c \tag{2.3}$$

where $\epsilon_{a,p}$ is plastic strain amplitude, ϵ'_f is fatigue ductility coefficient and c fatigue ductility exponent. While the Manson-Coffin equation describes the low-cycle high strain regime, the Basquin equation

$$\sigma_a = \Delta\epsilon_{a,e} E = \sigma'_f (2N)^b \tag{2.4}$$

where $\epsilon_{a,e}$ is elastic strain amplitude, σ'_f is fatigue strength coefficient and c fatigue strength exponent, describes the high cycle low strain regime. Summing up both equations, we get complete ϵ-N that is

$$\epsilon_a = \frac{\sigma'_f}{E}(2N)^b + \epsilon'_f (2N)^c \tag{2.5}$$

This equation can estimate the entire range of fatigue lives. Example of of ϵ-N curve and its construction can be observed in Figure 1.
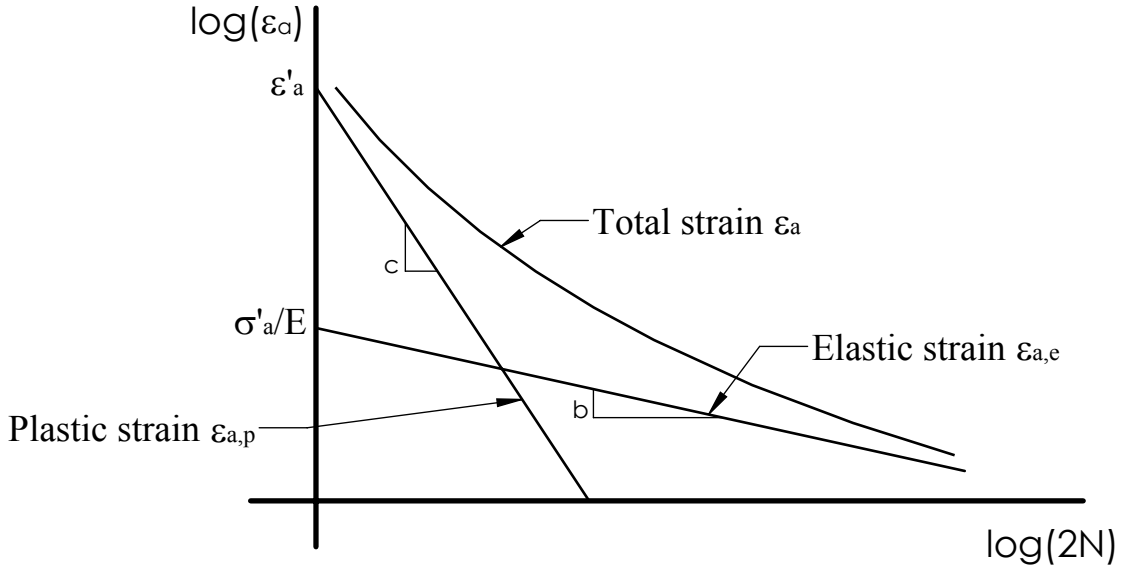
Figure 1: Example of ϵ-N curve and its construction

2.3 Thermo-mechanical fatigue

Thermo-mechanical fatigue (TMF) is caused by a combination of cyclic mechanical and thermal loading that is typical for turbine engines. The changing temperature during the loading can have more damaging effect on the structure than isothermal loading at the highest operating temperature. There are 2 types of loading:

in-phase(IP) and out-of-phase(OP). The former takes place when the maximum temperature and strain occur at the same time. The latter takes place when the maximum temperature and minimum strain occur at the same time. There are 3 different sources of failure in TMF that occur according to the type of loading(IP or OP). It is oxidation, creep and fatigue. When the structure undergoes IP loading, the creep is a driving fatigue mechanism. Conversely, when the OP loading dominates, the oxidation effects the fatigue life as it damages the component surface. It creates irregular surface that is ideal for the crack nucleation. There are many approaches that deal with TMF that are usually quite complex. In this thesis, one of them proposed by Nagode described.

3 LCF calculation methods

In this section 4 different method of LCF calculation are described in detail. These methods are historical GEAC method, SWT method, Landgrad method and Nagode's method.

3.1 Historical GEAC Method

Historical GEAC method is used as one possibility to predict LCF of the components. In this calculation, it is expected that we already know the load cycles that the component undergoes. Similarly, we expect that the stresses in the component from the elastic FEA for each time point of the load history are known. Firstly, a Manson-McKnight method is used for reduction of a multi-axial stress state to a uni-axial stress state. This uni-axial stress state is then recalculated to the Neuber parameter in order to include the effect of the mean stress in the calculation. Elastoplastic state of the material is estimated by Neuber formula. The steps of the procedure of this method are summarized as follows:

1. the reduction of a multi-axial stress state obtained from the elastic FEA to a uni-axial stress state

2. an elastoplastic stress estimation in turning points with the Neuber formula

3. a Neuber parameter calculation in order to include the mean stress effect

4. maximum number of equivalent cycles determination

3.1.1 Manson-McKnight Method

Once we have our load cycles defined and we performed an elastic FEA to get the stresses in the peaks of the load cycles, the Manson-McKnight method can be used to calculate uni-axial mean stress and stress amplitude of each cycle. Supposing that we obtained maximum and minimum stress tensors from elastic FEA for one load cycle:

$$\bar{\sigma}_{\max} = [\sigma_{\max_x} \ \sigma_{\max_y} \ \sigma_{\max_z} \ \tau_{\max_{xy}} \ \tau_{\max_{xz}} \ \tau_{\max_{yz}}] \tag{3.1}$$

$$\bar{\sigma}_{\min} = [\sigma_{\min_x} \ \sigma_{\min_y} \ \sigma_{\min_z} \ \tau_{\min_{xy}} \ \tau_{\min_{xz}} \ \tau_{\min_{yz}}] \tag{3.2}$$

we are able to transform these stresses to the equivalent uni-axial load cycle that should result in the same damage effect as the original multiaxial load cycle. The uni-axial elastic mean stress and stress amplitude are determined as:

$$\sigma_{a,FE} = \frac{\sqrt{2}}{4}[(\Delta\sigma_x - \Delta\sigma_y)^2 + (\Delta\sigma_y - \Delta\sigma_z)^2 + (\Delta\sigma_x - \Delta\sigma_z)^2 \tag{3.3}$$
$$+ \ 6\,(\Delta\tau_{xy}^2 + \Delta\tau_{yz}^2 + \Delta\tau_{xz}^2)]^{\frac{1}{2}}$$

$$\sigma_{m,FE} = SGN \ \frac{\sqrt{2}}{4}[(\Delta\sigma_x - \Delta\sigma_y)^2 + (\Delta\sigma_y - \Delta\sigma_z)^2 + (\Delta\sigma_x - \Delta\sigma_z)^2+ \tag{3.4}$$
$$+ \ 6\,(\Delta\tau_{xy}^2 + \Delta\tau_{yz}^2 + \Delta\tau_{xz}^2)]^{\frac{1}{2}}$$

where

$$\Delta\sigma_x = \sigma_{\max_x} - \sigma_{\min_x}, \ .... \tag{3.5}$$

$$\Delta\sigma_x = \sigma_{\max_x} + \sigma_{\min_x}, \ .... \tag{3.6}$$

Since the mean stress must always be positive, its sign is corrected according to:

$$SGN = SIGN[\Delta\sigma_x + \Delta\sigma_y + \Delta\sigma_z] \tag{3.7}$$

The maximum and minimum stress vectors, $\bar{\sigma}_{max}$ and $\bar{\sigma}_{min}$, are obtained from linear FEA and do not take into account a plastic behavior of the material. Hence, the elastic-plastic correction is then applied in order to obtain a real values of $\sigma_{a,FE}$ and $\sigma_{m,FE}$.

3.1.2 Neuber Correction

Neuber approximate formula is useful when stress results obtained from linear FEA need to be adapted to the elastoplastic behavior of the material. It is an alternative to the calculation of the elastoplastic stresses with nonlinear FEA. The main advantage of such a correction is a faster computation of the results compared to the

nonlinear FEM analysis. The assumption for use of this method is that the plastic stresses are concentrated only in a small area of the component.

The real stress according to the Neuber formula is located in the intersection of two curves: Neuber hyperbola and elastoplastic curve defined by Ramberg-Osgood relation (see Fig. 2).
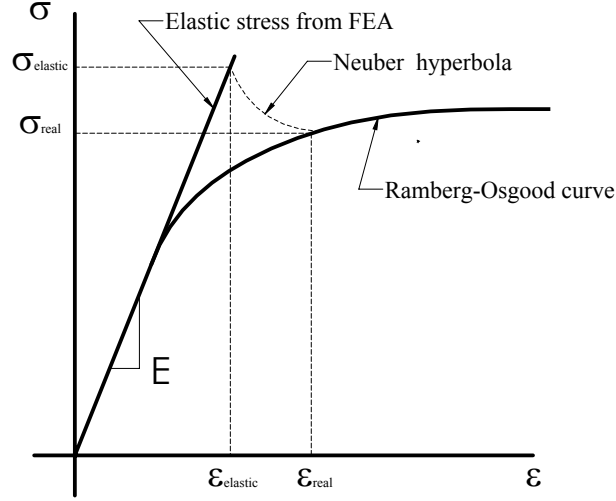
Figure 2: Correction of elastic FEA by use of Neuber formula

Equations that define these two curves are:

$$\frac{\sigma_{elastic}^2}{E} = \sigma_{real} \ \epsilon_{real} \tag{3.8}$$

$$\epsilon_{real} = \frac{\sigma_{real}}{E} + \left(\frac{\sigma_{real}}{K'}\right)^{\frac{1}{n'}} \tag{3.9}$$

respectively.

In our case, the calculation procedure is depicted in the plot in Figure 2 that shows how to correct stresses while a tension is applied. However, if the component is subjected to a large range of strains we can observe the reverse plasticity during the unloading. In such case, we should also correct the minimum stress and consequently also the alternating stress. The determination of the real (corrected) alternating stress, $\Delta\sigma_{real}$, can be seen in Figure 3.
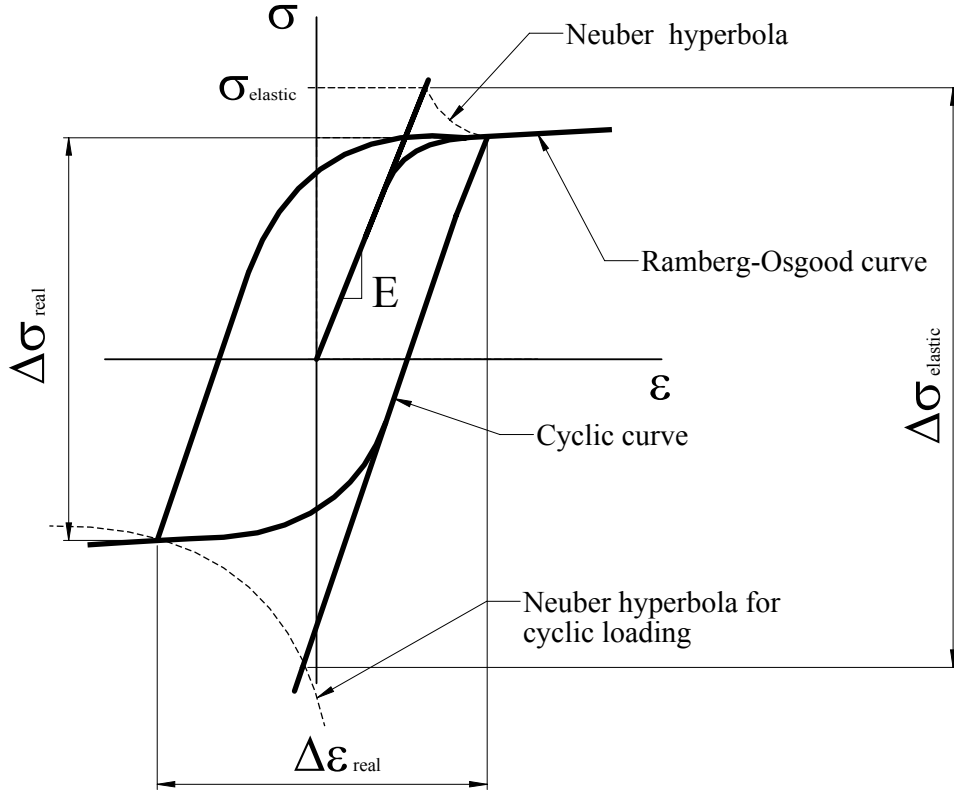
Figure 3: Correction of alternating stress obtained from FEA by use of Neuber formula

When calculating $\Delta\sigma_{real}$, the Neuber formula for cyclic loading is used for determination of the minimum real stress (see Fig. 3). Equation for Neuber hyperbola for cyclic loading is defined as follows:

$$\frac{\Delta\sigma^2_{elastic}}{E_{cyc}} = \Delta\sigma_{real} \; \Delta\epsilon_{real} \tag{3.10}$$

where E_{cyc} is the cyclic Young's modulus and $\Delta\sigma_{elastic}$ is equal to $2\sigma_{a,FE}$. We obtain the real stress-stain state in the point of the plot where the cyclic Neuber hyperbola intersects the cyclic curve. The cyclic curve is described by equation:

$$\frac{\Delta\epsilon_{real}}{2} = \frac{\Delta\sigma_{real}}{2\,E_{cyc}} + \left(\frac{\Delta\sigma_{real}}{2K'}\right)^{\frac{1}{n'}} \tag{3.11}$$

By combination of equations 3.10 and 3.11, we get an equation with one unknown variable which is $\Delta\sigma_{real}$:

$$\frac{\Delta\sigma^2_{elastic}}{E_{cyc}} = \Delta\sigma_{real} \left[\frac{\Delta\sigma_{real}}{E_{cyc}} + 2\left(\frac{\Delta\sigma_{real}}{2K'}\right)^{\frac{1}{n'}}\right] \tag{3.12}$$

16

Then, the real stress and strain amplitude and the mean stress of the cycle are:

$$\sigma_a = \frac{\Delta\sigma_a}{2} \tag{3.13}$$

$$\epsilon_a = \frac{\Delta\epsilon_a}{2} \tag{3.14}$$

$$\sigma_m = \sigma_{real} - \sigma_a \tag{3.15}$$

where σ_{real} is determined from Neuber formula for monotonic loading. The reason for this is that the loading starts as monotonic and begins to exhibit the cyclic behavior after some time. Thus, σ_{real} is derived from equation:

$$\frac{\sigma^2_{max,FE}}{E} = \sigma_{real}\left(\frac{\sigma_{real}}{E} + \frac{\sigma_{real}}{K}\right)^{\frac{1}{n}} \tag{3.16}$$

where $\sigma_{max,FE}$ is obtained from Manson-McKnight method as $\sigma_{max,FE} = \sigma_{m,FE} + \sigma_{a,FE}$ and K and n are parameters of the monotonic stress-strain curve.

3.1.3 Neuber Parameter

Neuber parameter is a stress amplitude that includes a mean stress effect to the calculation of LCF. It converts general cycle to the cycle with stress ratio $R = \sigma_{min}/\sigma_{max} = -1$. The Neuber parameter is calculated according to the following formula:

$$\sigma_{Neuber} = \sqrt{(\sigma_a + \sigma_m)\,\epsilon_a} \tag{3.17}$$

In order to determine a number of cycles to damage, the Neuber parameter is inserted into the equation for a curve from cyclic strain controlled fatigue testing(ϵ-N curve). This curve is also converted to Neuber parameter according to the same formula 3.17. The curve from the testing can be described by following equation:

$$\sigma_{Neuber} = M\,N^x \tag{3.18}$$

where N is a number of cycles to damage and M and x are coefficients obtained from the data interpolation.

3.1.4 Thermal loading effect on the LCF calculation

Thermal loading is an important point that should be taken into account during the LCF calculation if the component is subjected to the big changes in temperature. The prerequisite for this calculation is that we have temperature dependent S-N curves in the required temperature range available. Most frequently we have only

17

several S-N curves at our disposal and we need to use an interpolation to obtain S-N curves for some certain required temperatures. The Figure 4 shows how to determine fatigue life for some constant temperature if we do not have a S-N curve for it. Supposing that we have S-N curves for temperatures T_1 and T_2 available we look for S-N curve at constant temperature T so that the following statement is valid:

$$T \in <T_1; T_2> \tag{3.19}$$

Firstly, we compare our σ_{Neuber} with S-N curves at temperatures T_1 and T_2 and find corresponding maximum numbers of cycles N_1 and N_2. Then we plot these values in a plot where temperature T is on the horizontal axis and a logarithm of the number of cycles $logN$ is on the vertical axis. The desired fatigue life N is constructed by interpolation according to Figure 4.
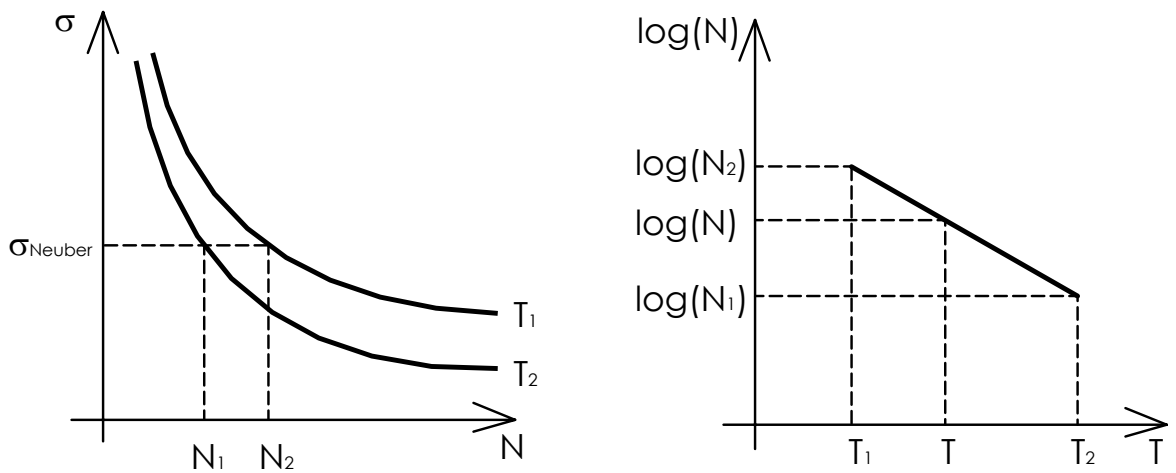
Figure 4: Determination of a fatigue life at the certain temperature T

However, the temperature is usually not constant during the load cycle and it can vary a lot with time. In such case we consider only temperature at maximum and minimum peak of the load cycle T_{max} and T_{min}. Firstly, the number of cycles for constant temperature T_{max} is calculated and than the same calculation is done for constant temperature T_{min}. Afterwards, we simply compare these two numbers and choose the lower one to make the life prediction more conservative.

3.2 Smith-Watson Topper method

The Smith-Watson Topper parameter (SWT) is widely used method that includes a mean stress correction in uniaxial loading. The SWT parameter is calculated as:

$$\sigma_{SWT} = \sqrt{(\sigma_a + \sigma_m)\epsilon_a E} \tag{3.20}$$

where σ_a and ϵ_m are stress and strain amplitudes. Once the SWT parameter for our cycle is determined, we can find a number of cycles to crack initiation by its insertion into equation for curve obtained from the strain controlled fatigue testing. The curve is defined as:

$$\sigma_{SWT} = {\sigma'_f}^2 (2N)^{2b} + \sigma'_f E \epsilon'_f (2N)^{b+c} \tag{3.21}$$

where σ'_f is fatigue strength coefficient, ϵ'_f is fatigue ductility coefficient, b is fatigue strength exponent and c fatigue ductility exponent. N is a desired number of cycles to crack initiation we are looking for.

3.3 Landgraf method

The Landgraf method is very similar to the determination of fatigue bz use of formula 2.5. The only difference in the way the mean stress σ_m is included into the fatigue life estimation. The assumption is that the mean stress influences only the Basquin equation (2.4) so that the formula for evaluating fatigue life N is described by equation:

$$\epsilon_a = \frac{\sigma'_f - \sigma_m}{E} (2N)^b + \epsilon'_f (2N)^c \tag{3.22}$$

3.4 A method proposed by Nagode

In order to predict the life of components that undergo TMF, a model proposed by Nagode is described. There are several factors that this model takes into consideration and makes the life evaluation more precise: a multiaxiality of the loading, elastoplastic behavior of the material, kinematic hardening and variable or constant temperature during the loading. These factors can play a significant role when one needs to perform proper fatigue life investigation since machine components are often subjected to multiaxial loading combined with loading beyond a yield stress. Hence, it is suitable to use the Nagode's model when a life evaluation of the structure with a complex stress-strain field is required.

Nagode suggested the following procedure for life estimation:

1. Transient thermal analysis using FEA in order to obtain temperature fields

2. Structural analysis using FEA in order to obtain stress fields - linear or non-linear

3. Conversion linear FEA results into nonlinear by use of the Neuber approximate formula in case the linear FEA was used

4. Stress strain modeling of complete hysteresis loops by use of rheological spring-slider model

5. Rain-flow counting of the stress history

6. Computation of equivalent cycle temperature for each cycle

7. Computation of the number of cycles to the crack initiation for each closed hysteresis loop

8. The damage estimation utilizing the Miner linear damage accumulation rule

In the following paragraphs, individual points of the procedure are described more in detail.

3.4.1 Transient thermal analysis

In order to obtain temperature fields at each time point of an investigated time interval, the transient thermal analysis can be carried out. It is based on the heat equation per unit volume which can be expressed as follows (assuming no mass transfer):

$$\rho c_p \frac{\partial T}{\partial t} - \Delta \cdot (k \Delta T) = q \tag{3.23}$$

where ρ is the density, c_p is the specific heat at a constant pressure, Δ is the nabla operator, k is the thermal conductivity coefficient and q is the heat generation rate per unit volume. We need to establish initial conditions for uniqueness of the solution. It can be done by either specifying an initial temperature distribution at the surface nodes that is already known or conducting a steady-state thermal analysis. This steady-state thermal analysis can be performed provided that the boundary conditions such as temperatures, heat fluxes or convection at the surface nodes are known. When initial conditions are set we can calculate temperatures at all the nodes that vary over the time. These temperature histories are then used as an input for the structural analysis.

3.4.2 Structural analysis

Once the temperatures in all nodes are obtained, structural analysis can be conducted by combining temperature and mechanical load histories. Provided that the boundary conditions and loads acting on the structure are known we can calculate the stress field at each time point using FEA. Linear or nonlinear analysis can be performed, assuming that the linear results are then recalculated using the Neuber approximated formula. If nonlinear FEA is carried out, an appropriate cyclic stress-strain relation should be used. The Ramberg-Osgood equation can be suitable; it describes material models that harden with rate-independent plastic deformation and shows a smooth transition between the elastic and plastic region

$$\epsilon = \frac{\sigma}{E(T)} + \left(\frac{\sigma}{K'(T)}\right)^{\frac{1}{n'(T)}} = g(\Delta\sigma, T) \tag{3.24}$$

where the coefficient E is the Young's modulus, K' is the cyclic hardening coefficient and n' is the cyclic hardening exponent. All these three parameters are functions of temperature.

Since the stresses are multiaxial, they must be converted from a multiaxial stress state to a uniaxial one. For this purpose it is convenient to use equivalent von Mises stress, $\sigma_{e,vM}$. However, $\sigma_{e,vM}$ does not exactly reflect the real load spectrum because it does not retain the negative stress values. In order to avoid this ambiguity of $\sigma_{e,vM}$, Bishop [5] suggested an alternative formula. According to Bishop, $\sigma_{e,vM}$ should be modified to signed von Mises stress. Therefore, the final output from the structural analysis is the signed Von Mises stress at each node and for each time point that is computed as follows:

$$\sigma_{e,svM} = SGN \frac{1}{\sqrt{2}}[(\sigma_1 - \sigma_2)^2 + (\sigma_2 - \sigma_3)^2 + (\sigma_3 - \sigma_1)^2]^{\frac{1}{2}} \tag{3.25}$$

where the symbol SGN indicates the sign of the principal stress with the largest magnitude. σ_1, σ_2 and σ_3 are the principal stresses.

Next, we use Neuber formula in order to transform the signed von Mises stress, $\sigma_{e,svM}$, gained from elastic FEA to real elastoplastic stress. The procedure can be seen in Figure 2 and is described by equations 3.8 and 3.9.

3.4.3 Stress-strain modeling

Since during the load history the plastic strains frequently occur a hysteresis phenomenon is modeled in the calculation. In addition, when temperature is changing

with time during the loading the material parameters such as Young's modulus and the yield stress are changing too. This causes that material exhibits so-called cyclic closure problem. It means that as the material is loaded and unloaded the hysteresis loops are no longer the same but they vary with time. In order to consider this phenomenon into calculation a modeling by use of hysteresis operator of Prandtl type is employed. In this approach, the play operator and the density function are utilized in order to describe the stress-strain relationship. The play operator simulates a rate-independent memory effect. It means that the output w of the operator is characterized by the current input and a previous input extrema, but not by the rate of the input. The operator is defined by the input function v that is equal to stress σ in our case and the threshold r that is a fictive yield stress in our case. A fictive yield stress is always positive. The output function of the operator w is then the strain ϵ. Such a modeling when the stress is an input function and the stress is an output function is called stress-controlled. The definition of the play operator according to [6] can be seen bellow. In operator form, we write, for $r \geq 0$,

$$w = \mathcal{F}_r[v] \tag{3.26}$$

Formally, the output function $w = \mathcal{F}_r[v]$ is for any piecewise monotone input function $v : [0, t_E] \to \mathbb{R}$ inductively defined by

$$w(0) = f_r(v_0, 0) \tag{3.27}$$
$$w(t) = f_r(v(t), w(t_i)), \qquad \text{for } t_i < t \leq t_{i+1}, \quad 0 \leq i \leq N - 1$$

with

$$f_r(v, w) = \max\{v - r, \min\{v + r, w\}\} \tag{3.28}$$

where $0 = t_0 < t_1 < ... < t_N = t_E$ is partition of $[0, t_E]$ such that the function v is monotone on each of the subintervals $[t_i, t_{i+1}]$. We call $\mathcal{F}_r$ the operator of scalar mechanical play or simply the play operator.

The stress-strain behavior is described by use of the operator of Prandtl type that utilizes play operator $\mathcal{F}_r[v](\text{t})$ as follows:

$$\epsilon(t) = P[\sigma, t] = \int_0^\infty \alpha(r, t) \ \sigma_\alpha dr \tag{3.29}$$

where $\alpha(r, t)$ is the Prandtl density function which is based on experimentally obtained data. We can obtain it from the cyclically stable isothermal cyclic curves. The argument of the operator is in square bracket to show that σ is a function of

another function. In order to solve the problem we need to approximate the integral. This is done by discretization, so that the equation 3.29 can be rewritten as

$$\epsilon(t_i) = \sum_{j=0}^{n_r} \alpha_j(T_i)\sigma_{\alpha j}(t_i) \tag{3.30}$$

The same relation can be written for the stress provided that different Prandtl density $\beta_j(T_i)$ is used:

$$\sigma(t_i) = \sum_{j=0}^{n_r} \beta_j(T_i)\sigma_{\alpha j}(t_i) \tag{3.31}$$

The relation 3.30 can be represented as the serially connected spring-slider model that can be seen in Figure 5.
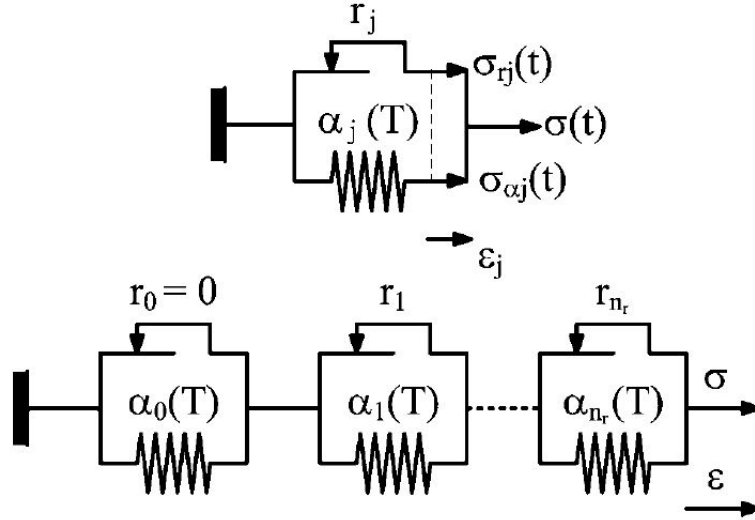
Figure 5: Rheological spring-slider model [1]

The spring-slider model consists of n_r segments when each of these segments represents an increment in the total elastoplastic strain. In equations 3.30 and 3.31, $\sigma_{\alpha j}(t_i)$ is determined as:

$$\sigma_{\alpha j}(t_i) = \max\left\{\sigma_{elastic}(t_i) - r_j, \min\left\{\sigma_{elastic}(t_i) + r_j, \frac{\alpha_j(T_{i-1})}{\alpha_j(T_i)}\sigma_{\alpha j}(t_{i-1})\right\}\right\} \tag{3.32}$$

Equation 3.32 corresponds to the play operator decribed in equation 3.28

3.4.4 Damage parameter

The damage parameter is continuously modeled using the modified hysteresis operator described by 3.28. The equation for the damage parameter is the same as the

equation for the SWT parameter (3.21), the only difference is that all the members in the equation are changing with time:

$$\sigma_{SWT} = \sqrt{(\sigma_a(t_i) + \sigma_m(t_i))\epsilon_a(t_i)E(T_i)} \qquad (3.33)$$

The strain life curves in this calculation are required for several temperatures, so that they can be interpolated for each temperature in the load history of the component. When we divide the interval $(0, \sigma_{SWT,max})$ to j members with a constant step Δr, the temperature dependent Prandtl densities of the discrete hysteresis Prandtl model are defined by the following relation:

$$\gamma_j = \frac{1}{4\Delta r}[d_{fj+1}(T) - 2d_{fj}(T) + d_{fj-1}(T)] \qquad (3.34)$$

where $d_f = 1/N$ is the cycle damage. The determination of σ_a, σ_m and ϵ_a is done through a special algorithm that is described in [1] in detail. This algorithm preserves the time sequence of decomposed σ_a, σ_m, ϵ_a and T. This is important in terms of the next calculation of the cumulative damage in each time point t_i. Simultaneously, the values of σ_{SWT} are calculated in each time step. The calculation of the damage $D(t_i)$ is carried out using the hysteresis operator as:

$$D(t_i) = \sum_{j=0}^{n_r} \gamma_j(T_i)\sigma_{\gamma j}(t_i) \qquad (3.35)$$

where the temperature dependent play operator is again defined as:

$$\sigma_{\gamma j}(t_i) = \max\left\{\sigma_{SWT}(t_i) - r_j, \min\left\{\sigma_{SWT}(t_i) + r_j, \frac{\gamma_j(T_{i-1})}{\gamma_j(T_i)}\sigma_{\gamma j}(t_{i-1})\right\}\right\} \qquad (3.36)$$

A cumulative damage in each time point is then:

$$D_{accum}(t_i) = \sum_{n=1}^{i} |D(t_n) - D(t_{n-1})| \qquad (3.37)$$

4 FEM Analysis

The scope of this section is the modal and static analysis of the impeller alternative design in the H80 engine and its results presentation. Modal analysis is done in order to find natural frequencies and corresponding mode shapes of the component. We investigate the natural frequencies of the unloaded impeller, only mechanically loaded impeller and thermally and mechanically loaded impeller. The modal analyzes are followed by a comparison of the natural frequencies for these three cases. The static analysis of the impeller is based on results obtained from the previously done thermal analysis. Input data for the thermal analysis are experimentally measured temperatures on the surface of the impeller.

4.1 Material

One considered option for the material of the impeller alternative design is a titanium alloy WL 3.7164 where the main alloying elements are aluminum and vanadium. Due to the low specific weight of the titanium alloys, it has a very good relationship between mechanical load-bearing capacity and weight. This material is therefore widely used in regions where the weight savings justify the use of an expensive material. Material properties used in the FEM analysis are shown in Figures 6, 7 and 8.
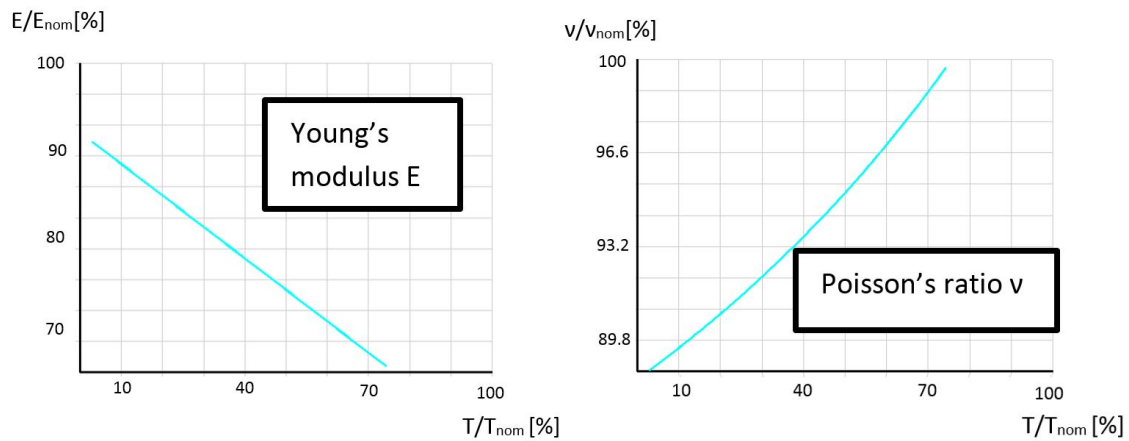
Figure 6: Young's modulus and Poisson's ratio of WL 3.7164 vs temperature
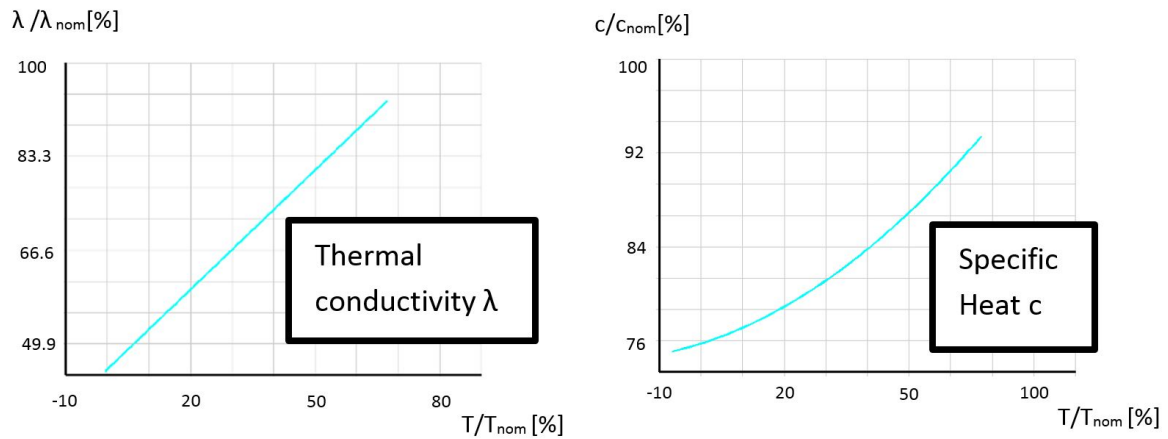
Figure 7: Thermal conductivity and Specific heat of WL 3.7164 vs temperature
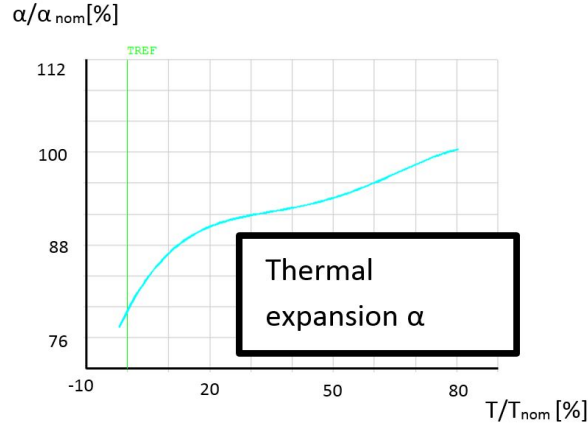
Figure 8: Thermal expansion of WL 3.7164 vs temperature

Since the impeller undergoes a rapid temperature changes, we also need to know how the material parameters change with the temperature. That is why all of them are plotted with respect to the temperature. All the curves in the plots are related to the reference values due to the GEAC restrictions. The density of WL 3.7164 is 4430 kg/m^3.

4.2 Modal analysis of the unloaded rotor blade

Firstly, the rotor blade of the impeller was analyzed in order to investigate its natural frequencies. The analysis was performed on the model that was not loaded.

4.2.1 Geometry

The geometry of the rotor can be seen in Figure 9. It consists of 16 main blades and 16 splitters. In order to achieve a simplified model that is faster to calculate, the symmetry of the rotor was utilized. So that only the sector with one blade and one splitter was analyzed as can be seen in Figure 9.

26
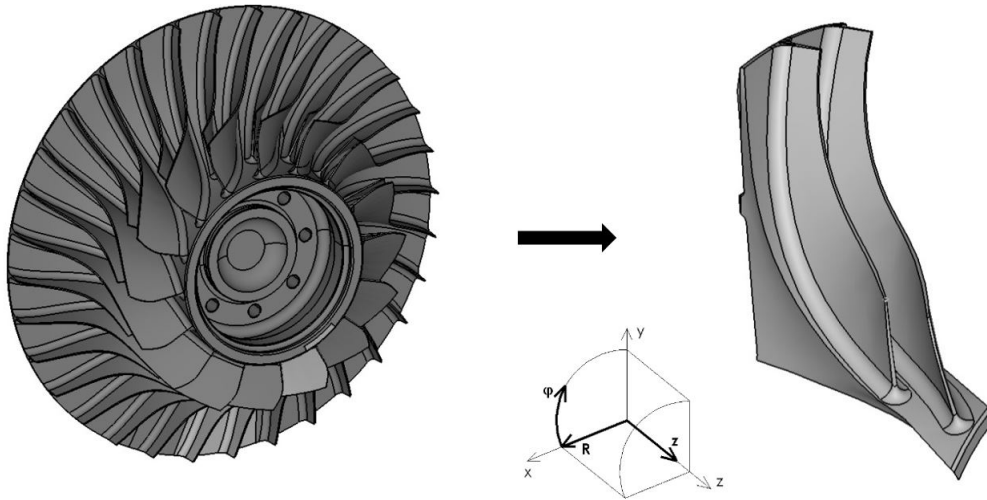
Figure 9: The whole impeller geometry(left) and its cyclic sector(right)

The sector angle is 22.5 degrees. Since in case of modal analysis, the behavior of the blades is the most crucial, the middle part of the rotor is treated as rigid. Therefore, it was removed and replaced by fixed boundary conditions. This assumption is only used in the first task as we want to simplify the model as much as possible. In the following part, modal analysis of the whole impeller is carried out. The material of the model is a titanium alloy and the geometry was edited in the Hypermesh software.

4.2.2 Mesh generation

The mesh was generated in Hypermesh software. An effort was made to use hexahedral elements as much as possible in order to increase the accuracy of the analysis and reduce the number of nodes. However, due to the complex geometry some segments of the model were meshed with tetrahedral, prism and pyramid elements. These segments do not include the blades that were fully meshed with the hexahedral elements. The meshed model can be seen in Figure 10.
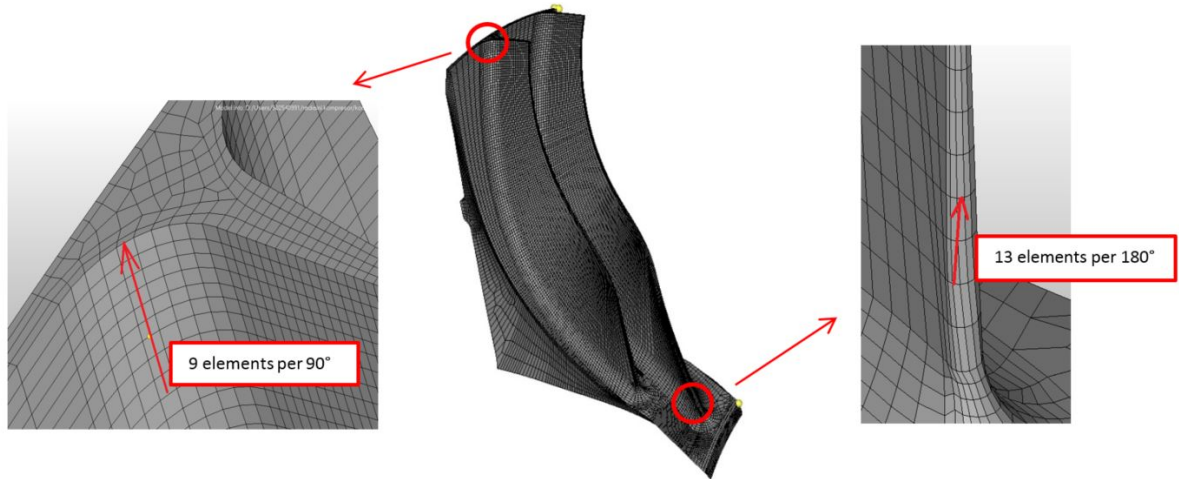
Figure 10: The mesh of the impeller cyclic sector model with a detailed view of trailing edge mesh (left) and leading edge mesh (right)

The whole model is meshed with the SOLID95 elements. This element type is the second order element that is suitable for modeling curved boundaries like in this model. It has 20 nodes but tetrahedral, prism and pyramid options are also available since some nodes can overlap as depicted in Figure 11. The total number of elements in the model is 116 375 and the hexahedral elements are filling 94% of the model.
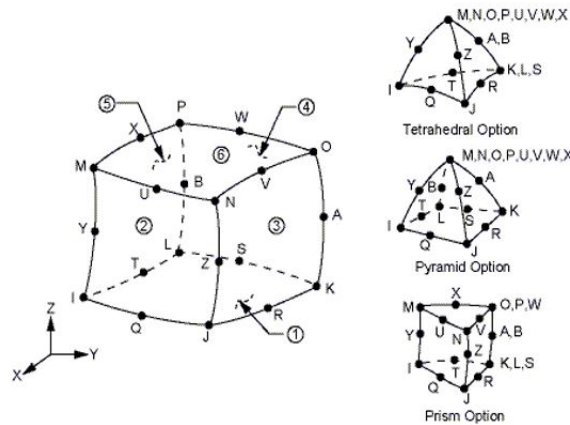
Figure 11: SOLID95 element geometry [4]

4.2.3   Boundary conditions

Since the modal analysis without any thermal or mechanical loads is required, only displacement constraints are applied. The component is fully fixed in the base

and there is applied symmetry on both sides of the sector, thus displacement in φ-direction at the sides equals 0 (see Figure 12).
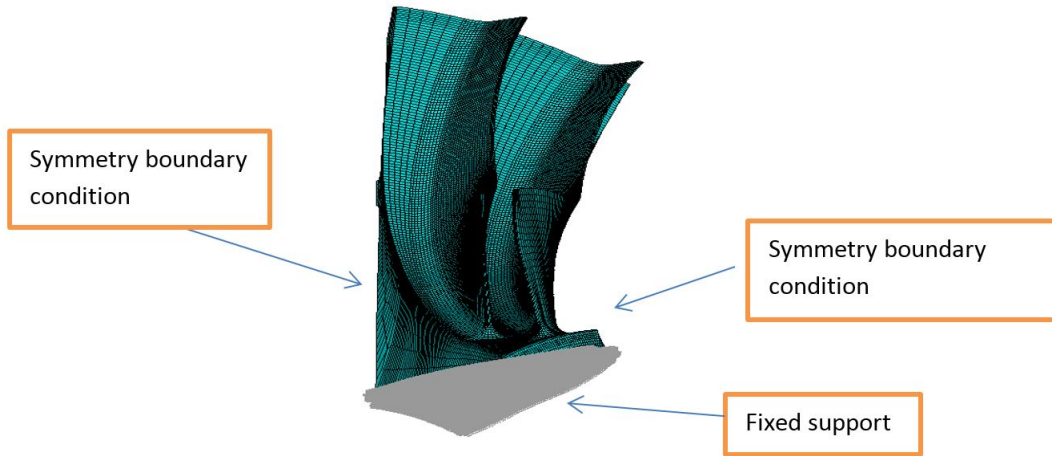
Figure 12: Boundary conditions for the modal analysis without loading

4.2.4 Results

Modal analysis was conducted in ANSYS software using the Block Lanczos mode-extraction method. There were 5 modes extracted and expanded in a frequency range from 0 to 10 000 Hz. The values of eigenfrequencies can be observed in Table 1. The modes shapes for the frequency sets from 1 to 5 are shown in Figure 13.

SET	FREQUENCY [Hz]
1	3623.7
2	4219.7
3	7434.3
4	9717.3
5	9965.6

Table 1: Natural frequencies of the impeller

From Figure 13, we can observe that the first mode shape that is associate with the frequency of 3624 Hz is the first bending mode shape for the main impeller blade. At the frequency of 4220 Hz we can find the first bending mode shape for the

29

splitter of the impeller. Frequencies of 7434 and 9717 Hz indicate the second and third bending mode shapes of the main blade. The second bending mode shape of the splitter is at the frequency of 9966 Hz.
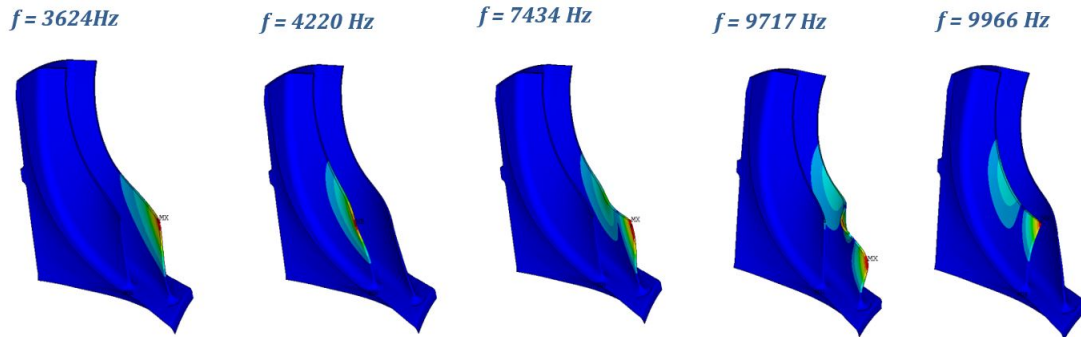
Figure 13: Mode shapes extracted for all the natural frequencies of the impeller

4.3   Thermal analysis of the rotor

The thermal analysis is carried out in order to obtain an input data for the structural analysis. The experimentally measured temperatures at discrete point are used as an input data for the thermal analysis. Temperatures at all nodes at each investigated time point are calculated as an output of this analysis.

4.3.1   Geometry and mesh of the model

For the thermal analysis, the model of the rotor is extended so that the inner part with the bolt and washer is also modeled (see Figure 14). In addition, parts of neighboring components are attached to the model in the front and back of the rotor. The sector angle is 45 degrees.
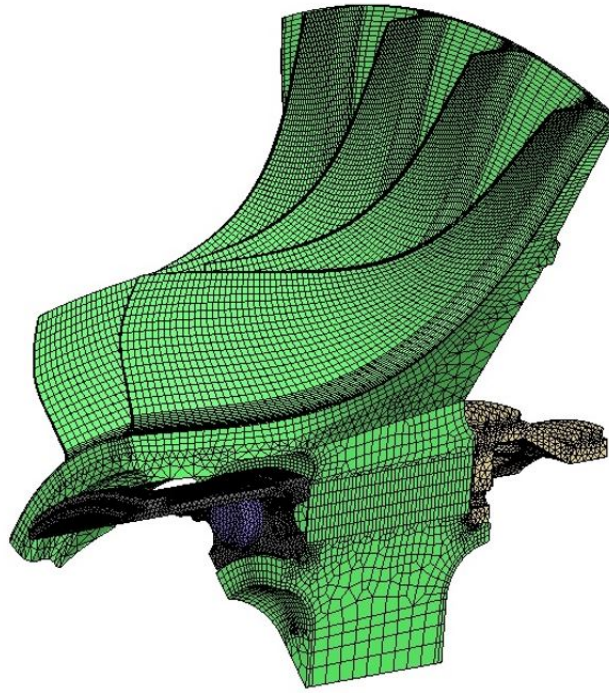
Figure 14: Impeller meshed model for the thermal analysis

The impeller is meshed with hexahedral SOLID90 thermal elements which are analogous to SOLID95 structural elements. The hexahedral elements fill the whole blades again and the tetrahedral thermal elements SOLID87 are used to mesh the other components since they are not as important as the blades. Contacts between all the components are modelled with CONTA173, CONTA174 and TARGET170 elements with temperature degrees of freedom.
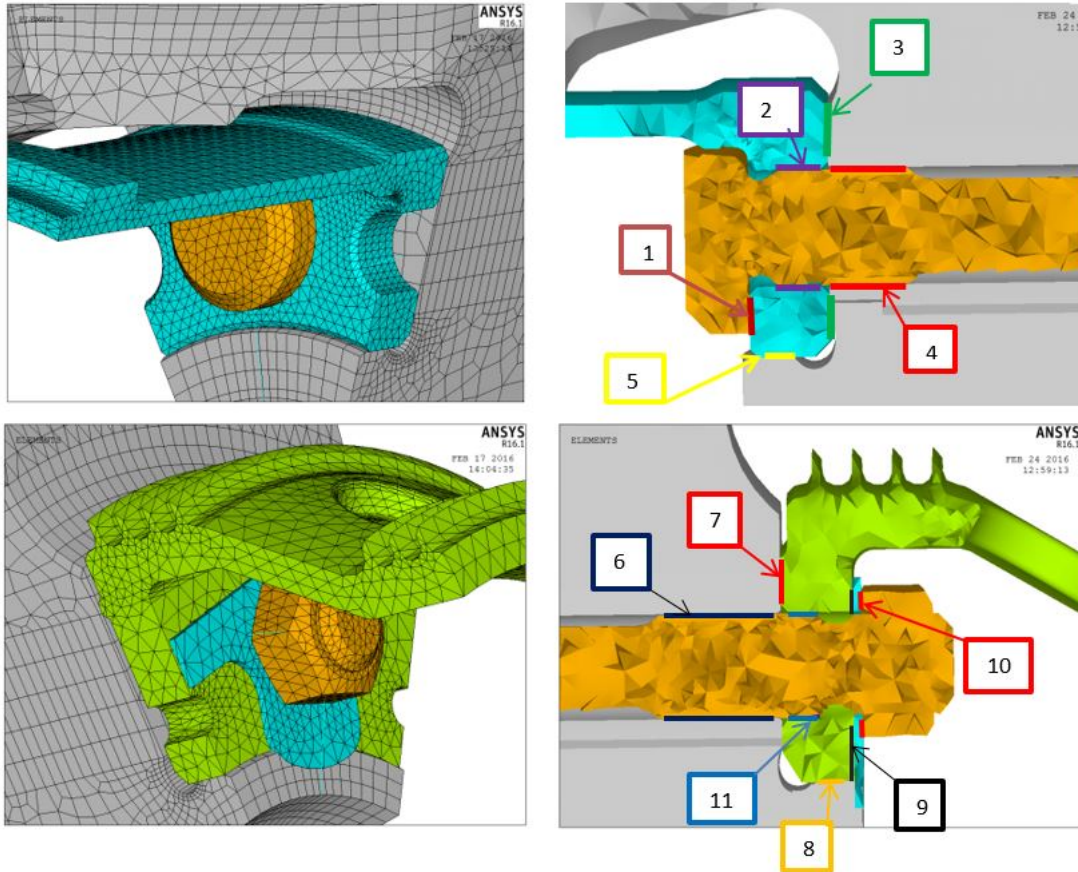
Figure 15: Contacts between the components in the model

All the contacts between the components are shown in Figure 15. They are modeled as 3D surface to surface asymmetric contacts. It means that all the contact elements are on one surface and all target elements are on the other surface on each contact. Flexible to flexible contact behavior is used for all the contacts. Keyoptions and real constants are set according to Table 2. The remaining real constants are default.

Contact	Element Type	K1	K2	K5	K10	K12	R10
1	CONTA174	1	1	3	2	1	0.195
2	CONTA174	1	1	0	2	1	0
3	CONTA174	1	1	3	2	1	0
4	CONTA173	1	1	0	2	0	0
5	CONTA174	1	1	0	2	1	0.00275
6	CONTA173	1	1	0	2	0	0
7	CONTA174	1	1	3	2	1	0
8	CONTA173	1	1	0	2	1	0.01
9	CONTA174	1	1	3	2	1	0
10	CONTA174	1	1	3	2	1	0
11	CONTA174	1	1	0	2	0	0

Table 2: Contact settings

In the Table 2, R10 is a real constant that specifies contact surface offset. Positive value offsets the entire contact surface towards the target surface. It can be automatically set by keyoption 5 that is explained later. The keyoption K1 selects degrees of freedom of the element. All the contacts have UX, UY, UZ and TEMP degrees of freedom which means that we can use them for structural and thermal analysis. The keyoption K2 indicates the contact algorithm. In our case, Penalty function is selected (K2 = 1). The keyoption K5 sets the behavior of the gap between two surfaces. It can automatically adjust the value of the contact surface offset (R10 real constant) according to the option we choose. The options are:

0 No automated adjustment

1 Close gap

2 Reduce penetration

3 Close gap/reduce penetration

The keyoption K10 sets contact stiffness update. If it is set to 2, it means that each iteration is based on current mean stress of underlying elements. Behavior of the contact surface is set by the keyoption K12. Only the options standard (K12 = 0) and rough (K12 = 1) are used. Standard contact surface behavior means that normal pressure between two mating surfaces is equal to zero if separation occurs. Rough contact is similar but there is no sliding possible so that the friction coefficient goes to infinity. Standard contact is set in the thread of the bolt with friction coefficient 0.15.

4.3.2 Thermal loading

Temperatures are mapped on the surface of the impeller according to the experimentally gained temperature fields. These temperature fields are obtained from the testing that is conducted on the rotating impeller. The impeller was accelerated and subsequently decelerated in the short time period. The rotational velocity was increased from 60% to 100% of the nominal speed in approximately 7 seconds during the acceleration. After 4 minutes the velocity was decreased back to 60% of the nominal speed. Dependency of the rotational velocity on time during the testing is shown in plot in Figure 16.
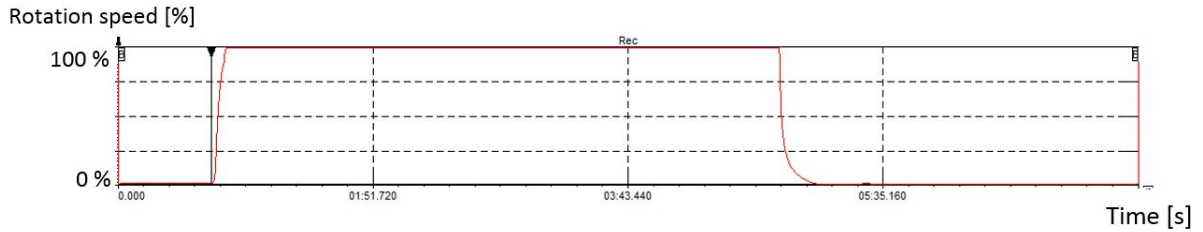
Figure 16: Rotational velocity vs time during the temperature field measurement on the impeller

The temperatures were measured using thermocouples mounted on the rotor surface while testing. The location of the thermocouples can be seen in Figure 17.
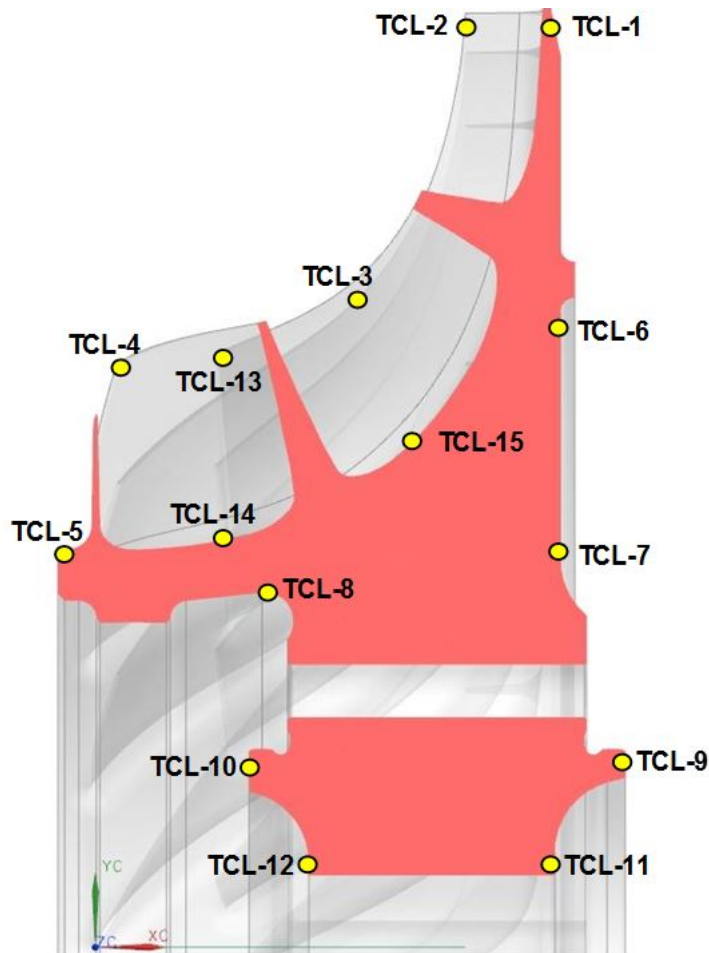
Figure 17: Distribution of the thermocouples on the impeller surface

Corresponding measured temperatures from the thermocouples for acceleration and deceleration are depicted in the plot in Figure 18. The onsets of acceleration and decelerations are marked with the dashed lines in Figure 18. The dashed lines also indicate time points with minimum and maximum temperature distributions during

the testing. Temperatures were measured at thermocouples TC1, TC2, TC3, TC4, TC5, TC6, TC7, TC9, TC11 and TC13. There were 6 time points chosen for the acceleration and 6 time points chosen for the deceleration. At these time points, temperature fields are used as an input for time - dependent thermal analysis.
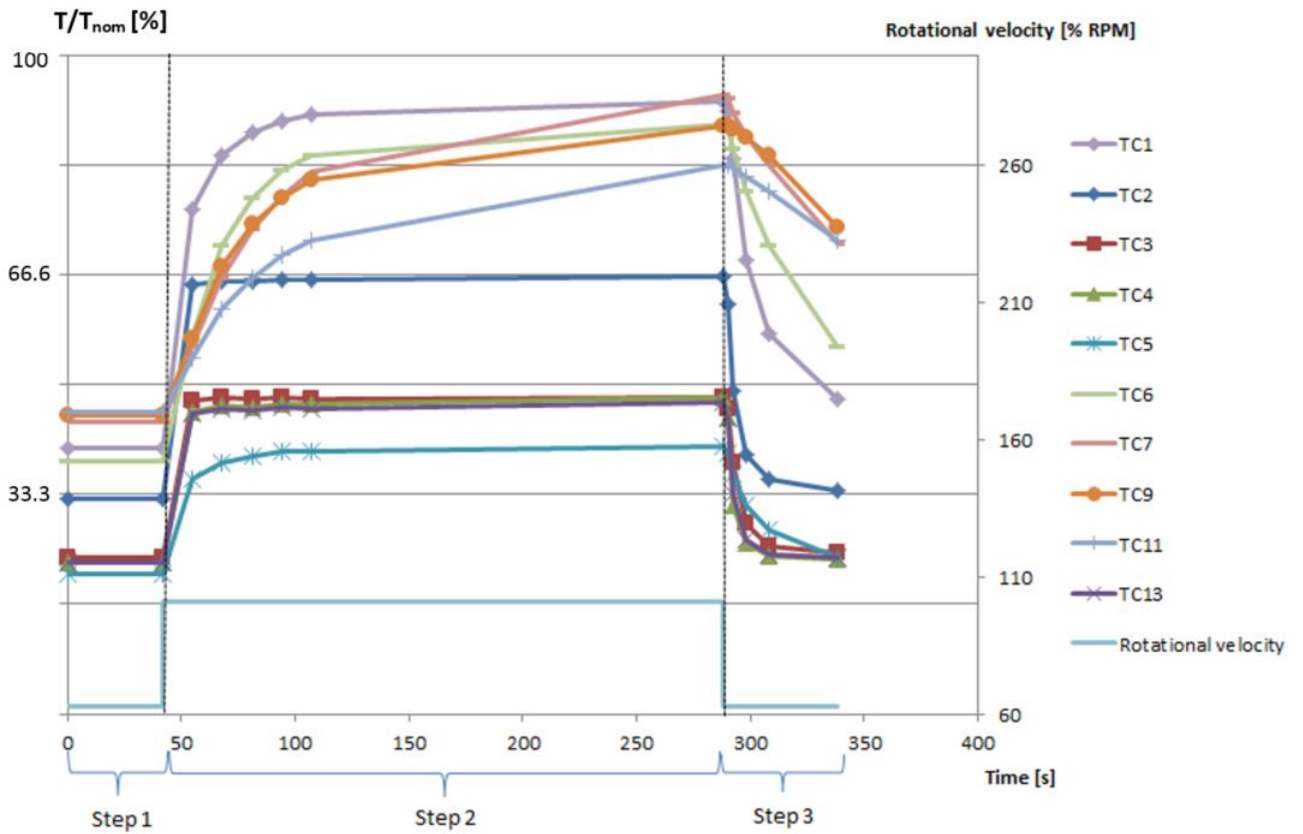
Figure 18: Temperatures measured by thermocouples on the rotor surface during the acceleration and deceleration

At each time point, measured temperatures are applied to the corresponding spots of the model and to its close surroundings. In Figure 19, we can see thermally loaded model in ANSYS. For the sake of simplicity, all the temperatures are loaded into ANSYS in a form of a table.
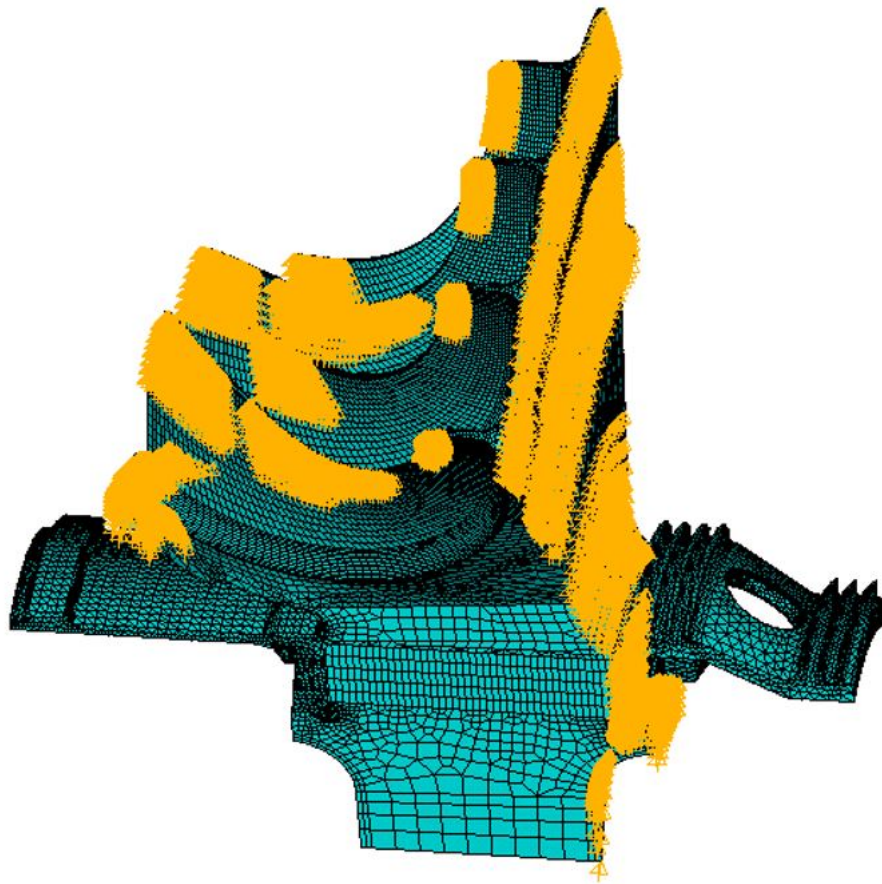
Figure 19: Temperature applied on the impeller model in ANSYS

4.3.3 Results

Thermal analysis is performed in three time steps. In the first step, the temperature field associated with the speed of 60% of the nominal speed was applied on the model. The second step corresponds with the acceleration. This step was divided into six substeps. At each substep a new temperature field is loaded from the preprocessed. The third step corresponds to the deceleration that is also divided into 6 substeps. The results of the thermal analysis at the beginning of the acceleration (i.e. 60% of the nominal speed) and at the end (i.e. 100% of the nominal speed) are shown in Figure 20
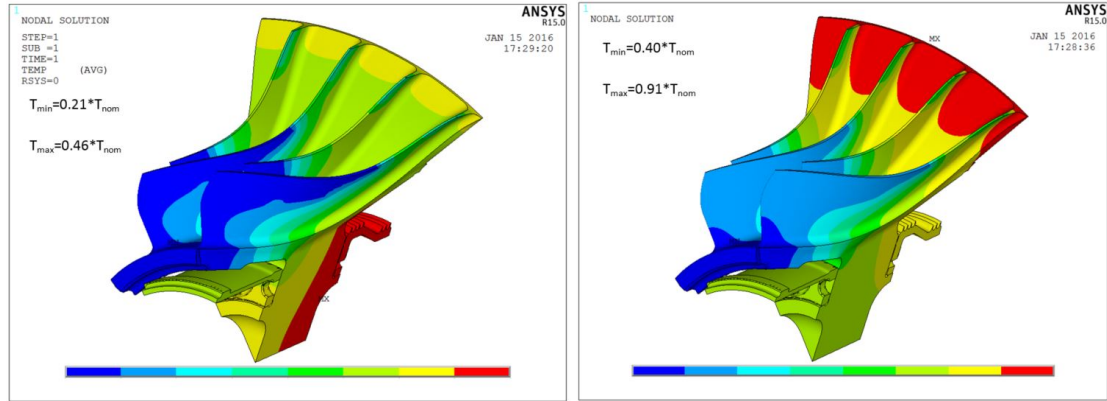
Figure 20: Temperature distribution on the impeller at the speed of 60% of the nominal speed(left) and at the speed of 100% of the nominal speed

4.4 Static and modal analysis of the loaded rotor

4.4.1 Geometry and mesh of the model

For the static and modal analysis, the same mesh and geometry are used for the thermal analysis (see Figure 14). However, the thermal elements had to be replaced by structural elements; thus, SOLID186 and SOLID187 elements are used. Contacts between the components are again meshed with CONTA173, CONTA174 and TARGET170 elements. The settings for the contact elements are the same as for the thermal analysis.

4.4.2 Boundary conditions and loading

Boundary conditions for the static analysis are shown in Figure 21. The pressure caused by hot gas is acting on the rear side of the impeller in the axial direction. In addition, the whole model is loaded by rotational velocity that varies with time in steps according to Figure16. It means that the first and third step correspond with the speed of 60% of the nominal speed and in the second step velocity of 100% of the nominal speed was applied. Consequently, the corresponding temperatures obtained from previous time-dependent thermal analysis are applied to all nodes.
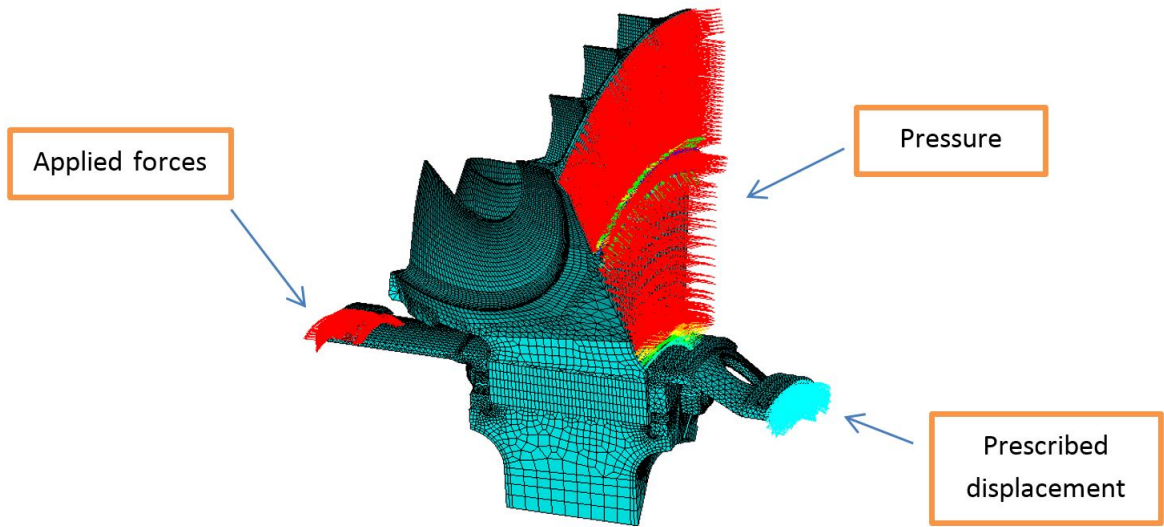
Figure 21: Applied load on the model for the static analysis

Thermal loads and rotational velocity are applied in the same steps as in the thermal analysis. Moreover, there are applied forces and prescribed displacement on the components attached to the impeller according to Figure 21. The cyclic symmetry utilized for sector angle of 45 degrees. The contacts between all the components are modelled with surface-to-surface contact option in ANSYS that includes friction between the surfaces again. The pure penalty contact algorithm is also used for these contacts. In order to simulate the pretension of the bolt, the PRETS179 elements with one translation degree of freedom are utilized in the cross-section of the bolt.

4.4.3 Static analysis results

The results of the static analysis can be observed in Figures 22 and 23. We can see the comparison of von Mises stress at the beginning and at the end of the second step. At the beginning of the step 2, the speed is already 100% of the nominal speed but the temperatures are still the same as in the first step. At the end of this step, the speed remains the same and temperatures increase to their maximum. Thus, in Figures 22 and 23, we can see the influence of the temperature change on the von Mises stresses.

Figure 22: Von Mises stress at the speed of 100% of the nominal speed loaded with minimum temperature field
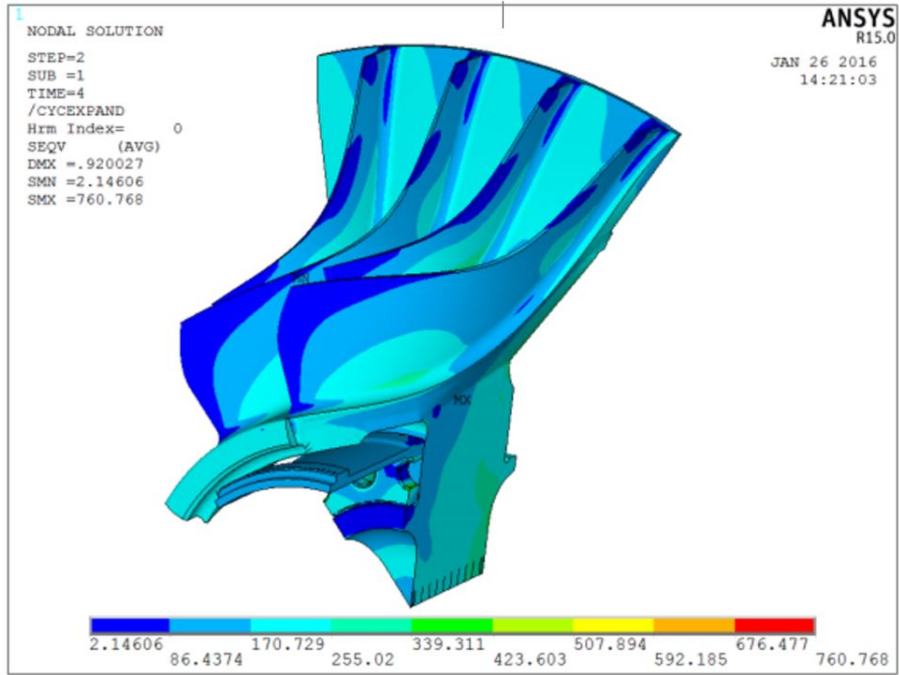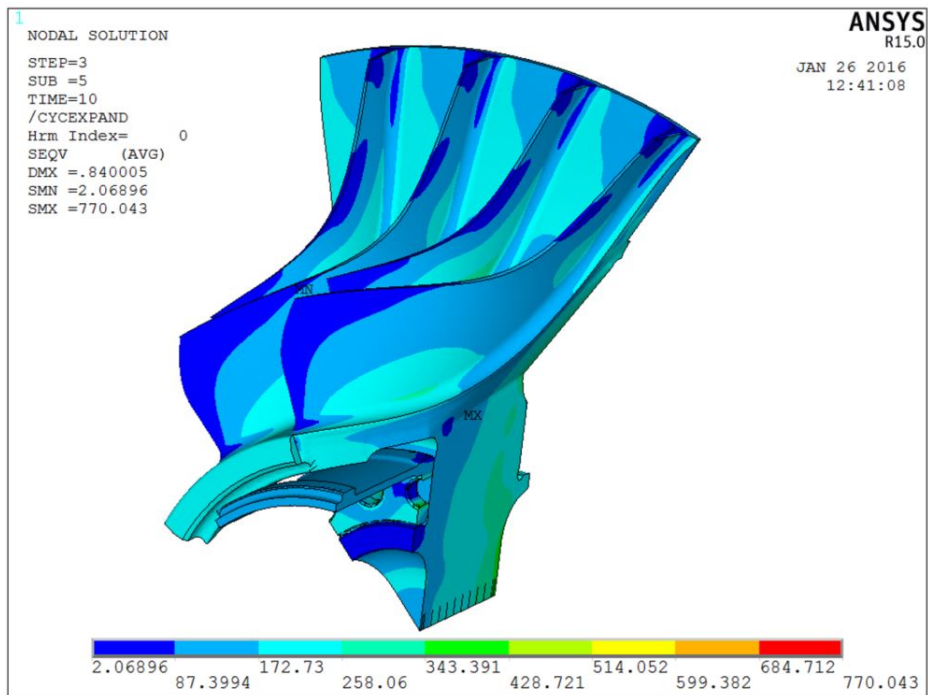

Figure 23: Von Mises stress at the speed of 100% of the nominal speed loaded with the maximum temperature field

However, there is only minor change; more detailed view can be seen in the plot

in Figure 24 where the dependency of von Mises stress at node 1461567 on time is plotted. σ_{ref} in the plot is equal to von Mises stress at speed of 100% of the nominal speed RPM and minimum temperature field.
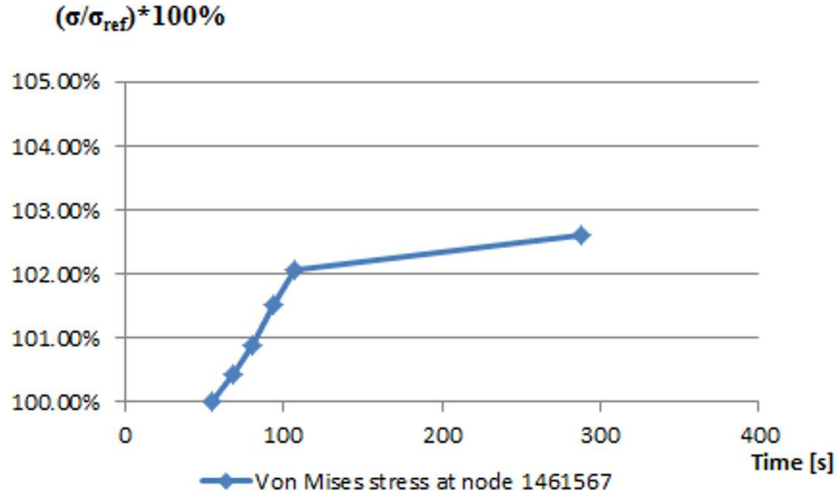
Figure 24: Von Mises stress vs time at node 1461567 during the temperature increase in load step 2

The critical locations on the impeller are shown in Figure 25 and their description is in Table 3.

Location	Node No.	Von Mises Stress
1	1461567	770.04
2	1461799	685.95
3	1466581	506.55

Table 3: Nodes with the highest von Mises stress

The node 1461567 with the highest von Mises stress is located at the top of the hole for the bolt. The increase in von Mises stress due to the temperature change at this node is only 2.6%. Therefore, we can conclude that the stress increase caused by growing temperatures can be neglected in this quasi-static analysis. However, care should be taken because in case we performed transient thermal analysis results could be different, since we would also take into account time-dependency of the analysis.

40
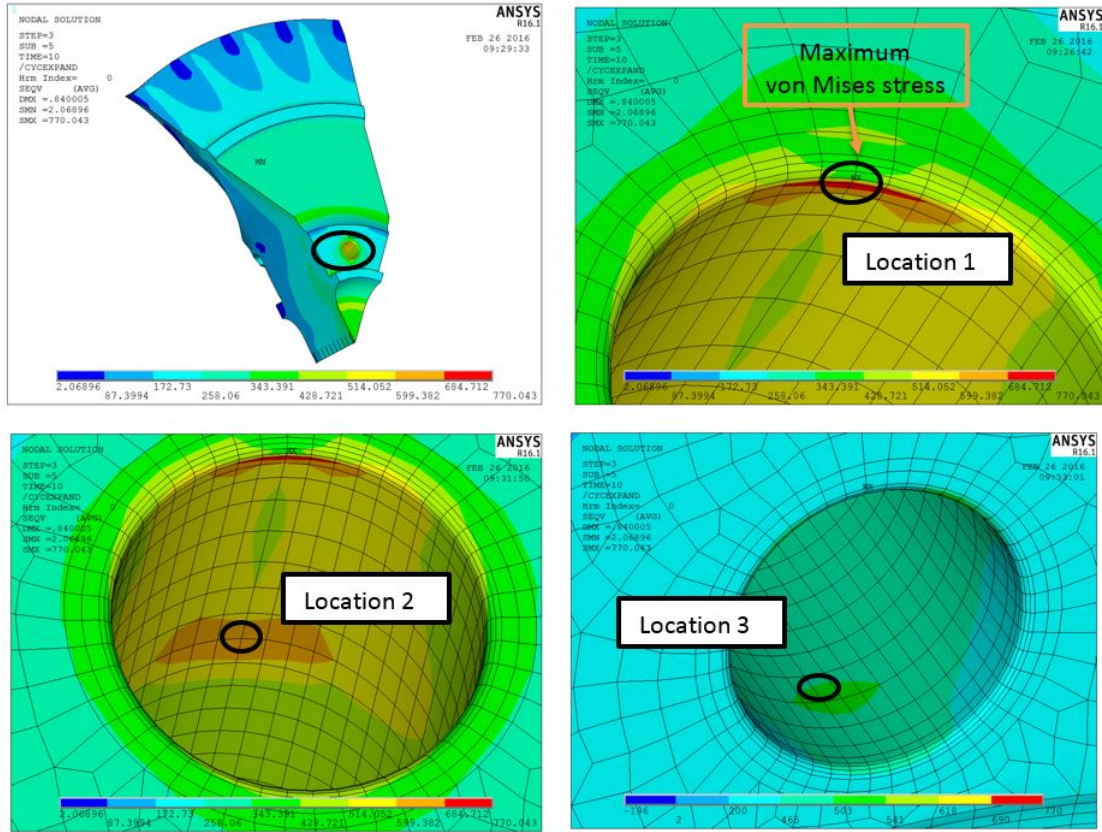
Figure 25: Critical locations with the highest von Mises stresses

4.4.4 Modal analysis results

Perturbed prestressed modal solution is performed on the impeller cyclic-sector model. The perturbed modal cyclic symmetry analysis includes the initial prestressed condition obtained from the previous linear static analysis. Thus, stresses from pressure, centrifugal loading caused by rotational velocity and thermal loading are included in the solution. The modal analysis without thermal loading is also conducted in order to investigate the influence of the temperature on the natural frequencies. The Block Lanczos eigensolver was used to extract 7 modes for harmonic index 0. The results are shown in Table 4. The results for the loaded impeller without thermal loading are shown in Table 5. Mode shapes for the first 4 natural frequencies are depicted in Figure 26. We can see that the eigenfrequencies of the prestressed impeller are higher than the corresponding eigenfrequencies we have got when we analyzed only the unloaded blade. This meets our expectations since the stiffness is getting higher during the loading. When we added the thermal loading the natural frequencies decreased. This also corresponds to the expectation. In the prestressed analysis, some extra eigenfrequencies occurred that are caused by two

41

SET	FREQUENCY [Hz]
1	4073.1
2	4094.9
3	4618.8
4	4620.5
5	5389.7
6	7497.9
7	7614.6

SET	FREQUENCY [Hz]
1	4174.3
2	4198.1
3	4782.6
4	4785.1
5	5596.8
6	7705.1
7	7825.3

Table 4: Natural frequencies of the loaded impeller (harmonic index = 0)

Table 5: Natural frequencies of the cold loaded (harmonic index = 0)

factors. Firstly, the model and mesh are different compare to the model in the first task. The sector angle is two times bigger and there are additional components attached to the impeller. Secondly, cyclic symmetry is used in this analysis instead of symmetry boundary conditions that are used in the first task.
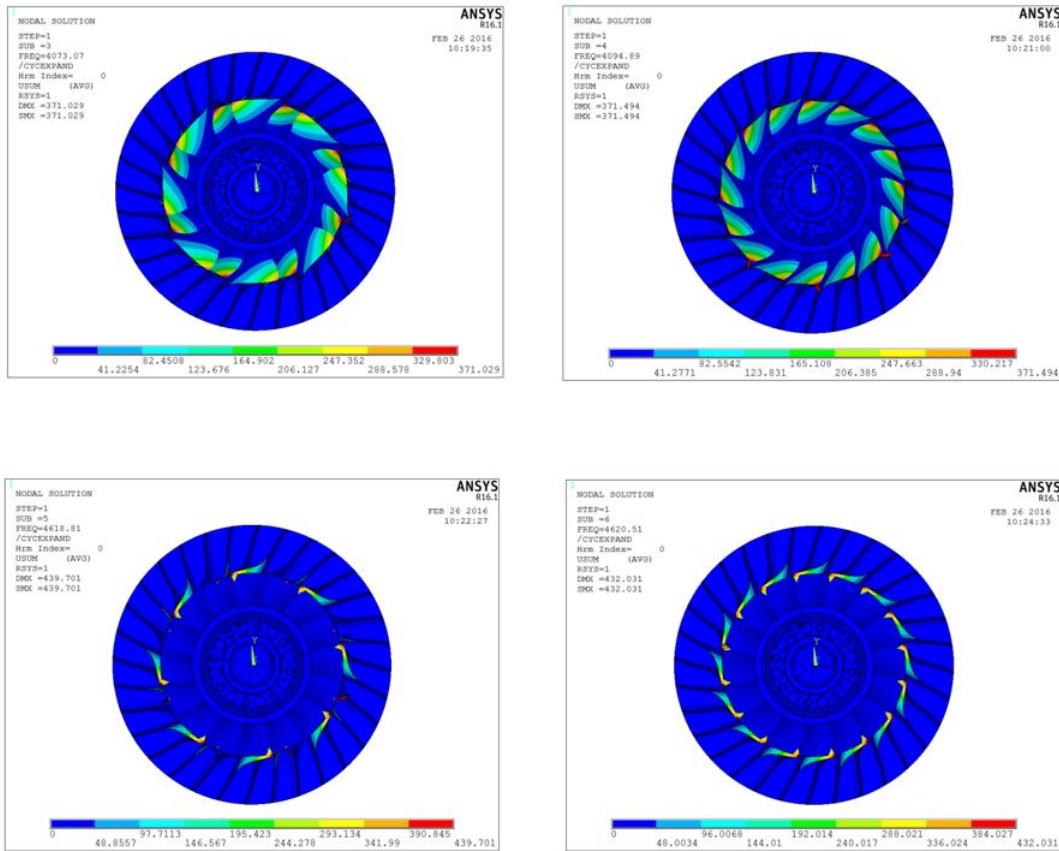

Figure 26: Mode shapes of the first 4 eigenfrequencies of the thermally and mechanically loaded impeller

42

In Figure 27, we can observe the comparison of natural frequencies belonging to the unloaded model, loaded impeller without thermal loading and fully loaded impeller. It can be seen that for the higher frequencies the natural frequencies of unloaded and fully loaded impeller are comparable. It is caused by the fact that the thermal load decreases the natural frequencies back to the initial value. Note, that there are not all the eigenfrequencies for the unloaded rotor since some modes do not exist in the simplified model.
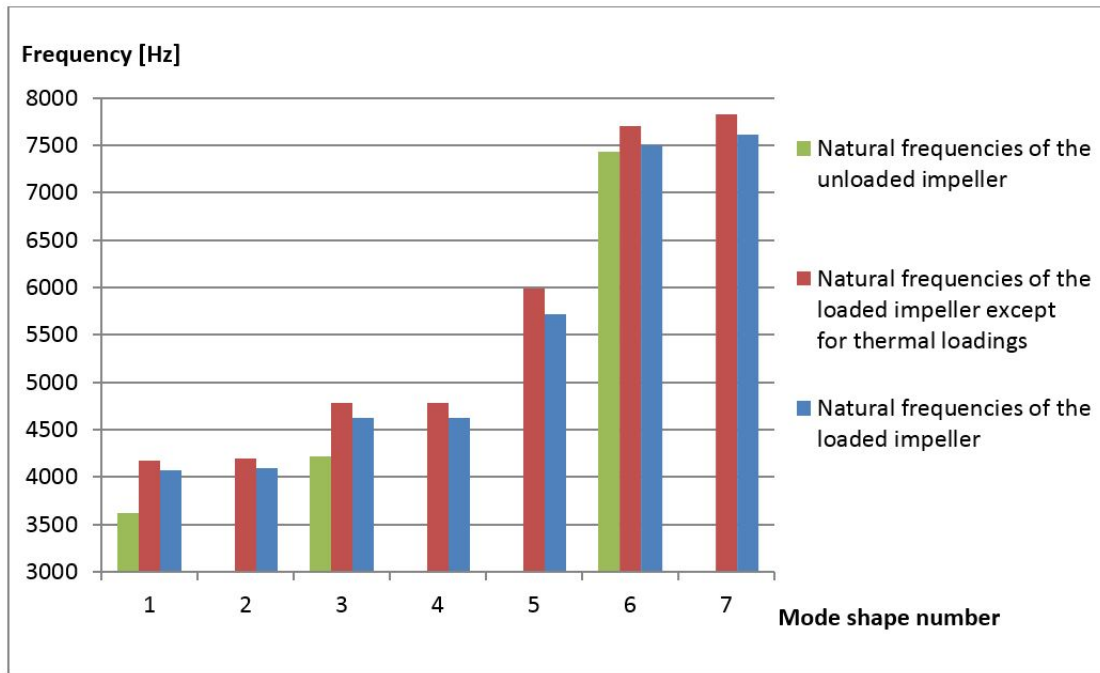
Figure 27: Comparison of eigenfrequencies of unloaded, structurally loaded and both thermally and structurally loaded impeller

5 Fatigue Life Assessment

This section describes the low cycle fatigue(LCF) calculation of the impeller based on the FEA results. The LCF evaluation is performed by the use of three different methods. Namely, it is the SWT method, Landgraf method and historical GEAC method. For the fatigue life analysis we need three types of input data in order to obtain the results. It is a load history of the component, elastic stress response to the loading obtained from the FEA results and the material properties. All of them are described bellow in more detail except for the FEA results that were already described in the previous section 4.

43

5.1 The loading history

The loading history of the impeller can be seen in Table 6 and plotted in Figure 28. There are different flight operations that the engine experiences and their numbers of occurrence stated. It is basically an output from the rainflow counting.

Cycle No.	Cycle	ω_{min} [%]	ω_{max} [%]	Occurrence per cycle
1	**Take-off Overshoot**	0	104.5	1
2	**Flight Idle**	60	96	1
3	**Recurrent take-off**	60	104.5	0.05
4	**Limiters test**	0	95	0.22

Table 6: The loading history of the impeller

The flight operations are always specified by the maximum and minimum rotational velocity during the cycle as these two values are crucial for the fatigue life calculation. In addition the structure is permanently subjected to a constant load caused by the bolt pretension.
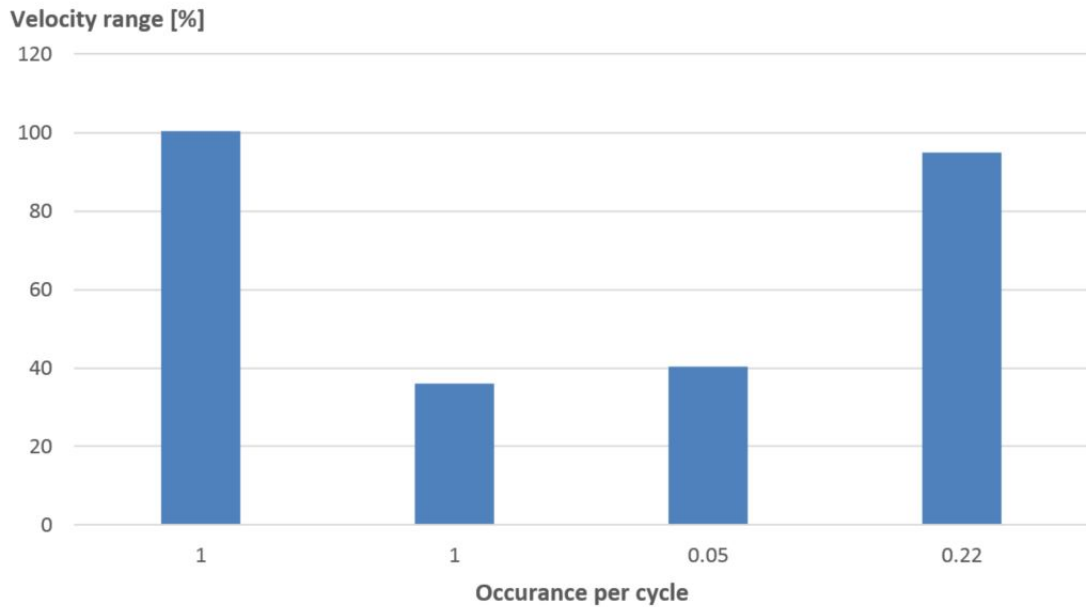

Figure 28: The loading history of the impeller

44

5.2 Material Properties

In this section, the material properties requires for LCF prediction are presented. All the material curves are related to reference values because of the GEAC restrictions.

5.2.1 Cyclic curve

For the fatigue life calculation, we need to know cyclically stable cyclic stress-strain curves for several temperatures. The cyclically stable curves that we have were measured at 3 different temperatures: 23^oC, 240^oC and 265^oC . Each of them is gained by an interpolation of 12 points. The points represent peaks of stabilized stress-strain hysteresis loops. Such a hysteresis loop is depicted in Figure 29 where $[\epsilon_{alt}; \sigma_{alt}]$ are the coordinates of each point that we needed for the interpolation.
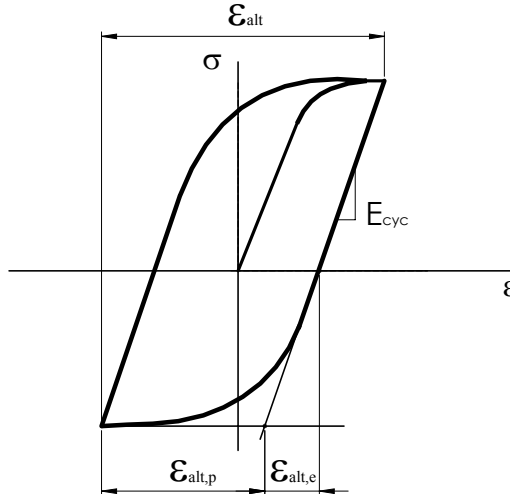
Figure 29: Example of hysteresis loop the data for cyclic curve were taken from

In order to obtain the hysteresis loops cyclic strain-controlled loadings at several strain levels were performed. A schematic chart of such a strain loading in time is in Figure 30. It can be observed from Figure 30 that the loading is for $R = -1$. The material specimen response to the applied cyclic strain loading can be schematically seen in Figure 31. As the specimen is loaded the alternating stress is decreasing until the specimen fails after a certain number of cycles N. Such trend is called material softening since the material is loosing its initial strength. On the other hand if the process was opposite and the alternating stress was increasing the process would be called hardening. The hysteresis loop we use for our cyclically stable curve is the one that we measure after $N/2$ cycles.
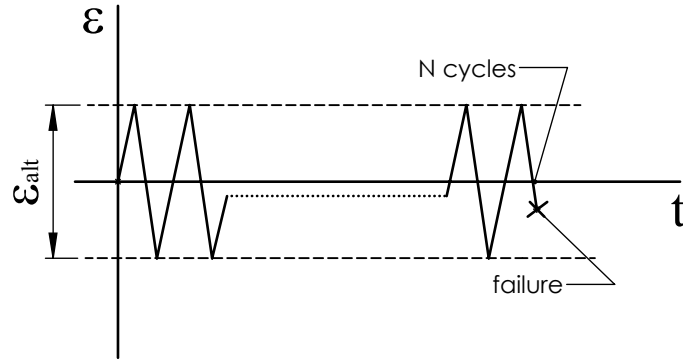
Figure 30: Example of a strain - controlled cyclic loading
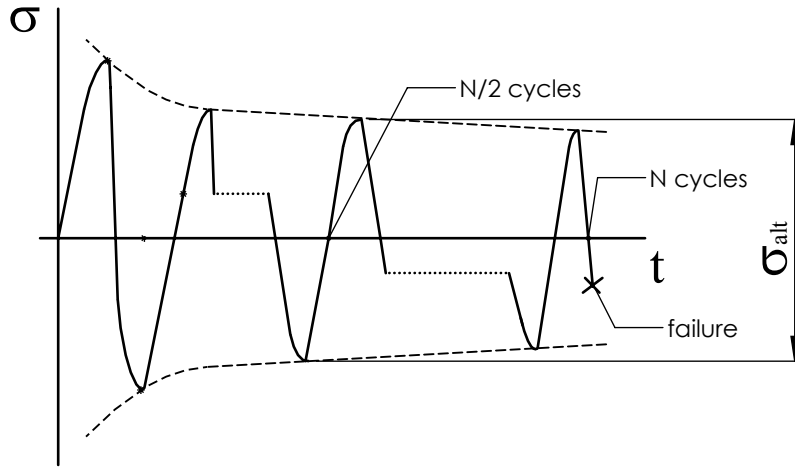
Figure 31: Example of material stress response to strain - controlled cyclic loading

Since the cyclic curve is dependent on temperature and deformation rate, all the points were measured isothermally and with constant frequency $v = 0.167 Hz$ They were then interpolated by a curve with an equation:

$$\sigma_{alt} = A \left(\epsilon_{alt,p} \right)^B \tag{5.1}$$

Where ϵ_{ap} is a plastic part of the alternating strain. By comparing equation 5.1 with equation 3.9, we can determine coefficients K' and n' for each temperature.

$$K' = A \tag{5.2}$$

$$n' = \frac{1}{B} \tag{5.3}$$

These coefficients define our cyclic curves. The plot of the cyclic curve for temperature 240 ^oC can be seen in Figure 32.
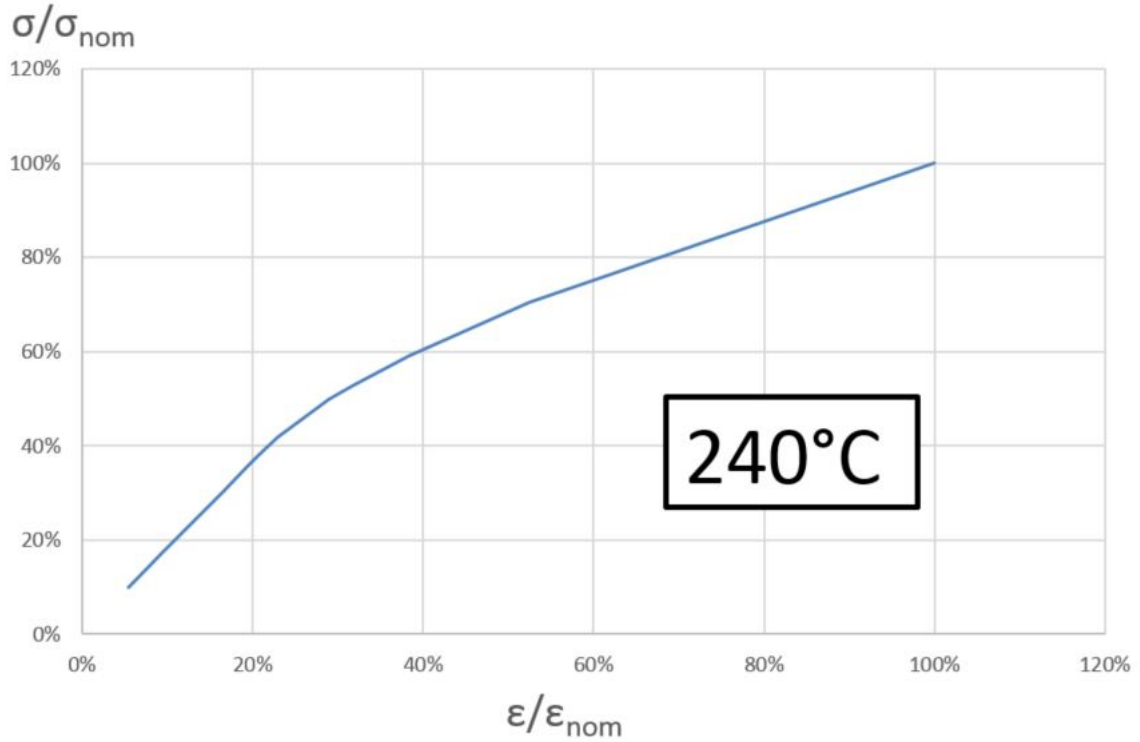
Figure 32: The cyclic curve for temperature 240 ^{o}C

5.2.2 Strain-Life curve

The other material parameters we necessarily need for the LCF calculation are the parameters that the $\epsilon-\mathrm{N}$ curve is described with. The $\epsilon-\mathrm{N}$ curve is described with equation 3.21 thus we need to get σ'_f, ϵ'_f, b and c. We obtain these constants from the same testing as for the cyclic curve. During the testing both the elastic and the total strains are measured. The total strain ϵ_{alt} is measured directly by a tensometer mounted on the specimen. Whereas the elastic strain is derived from

$$\epsilon_{alt,e} = \frac{F}{A} \tag{5.4}$$

provided that the load force F and cross-section A are continuously measured during the testing. The plastic strain is then calculated as $\epsilon_{alt,p} = \epsilon_{alt} - \epsilon_{alt,e}$. The strain life curve is gained as a superposition of two curves. It is an elastic strain-life curve and plastic strain-life curve. Both of these curves were gained from the interpolation. The elastic strain- life curve extrapolates the points with coordinates $[N; \epsilon_{alt,e}]$ and the plastic strain life curve extrapolates the points with coordinates$[N; \epsilon_{alt,p}]$. N is a number of cycles to failure of each specimen, $\epsilon_{alt,e}$ is an elastic alternating strain and $\epsilon_{alt,p}$ is a plastic alternating strain. The equation for the final strain life curve

is:

$$\epsilon_{alt} = \epsilon_{alt,e} + \epsilon_{alt,a} = A \ N^a + B \ N^c \tag{5.5}$$

Where the first member on the right side of the formula represents the elastic part of the strain and the second member represents the plastic part of the strains. Constants A, B, a, c are obtained from the interpolation. The parameters σ'_f, ϵ'_f, b and c are obtained by comparison equation 5.5 with equation 18 as follows::

$$\sigma'_f = A \ \frac{E_{cyc}}{2^{b+1}} \tag{5.6}$$

$$b = a \tag{5.7}$$

$$\epsilon'_f = \frac{B}{2^{c+1}} \tag{5.8}$$

$$c = c \tag{5.9}$$

The ϵ-N curve for the used material and temperature 240 ^oC is depicted in Figure 33.
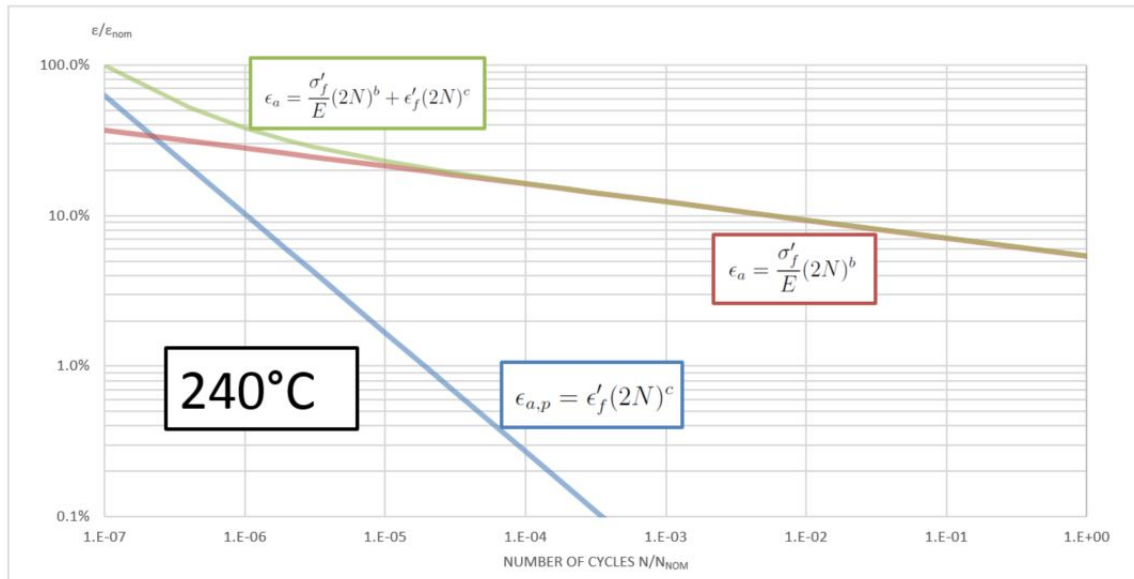
Figure 33: ϵ-N curve for temperature 240 ^oC

5.3 Fatigue assessment using SWT method

5.3.1 The input data implementation

Fatigue assessment using SWT method is performed in the PragTic software. The stress tensor at each node of the impeller FEM model for each time point of the loading history is implemented to PragTic. Since the analysis was elastic the stresses at each time points are proportional to rotational velocity squared ω^2. Therefore

only one stress result file is uploaded to PragTic and the remaining stress tensors are only multiples of the original stress file. This simplification can be only used considering that the loading of the impeller is controlled mainly by the rotational velocity and that the change in stress caused by the temperature influence is insignificantly small. In addition care should be taken because there are also stresses caused by bolt pretension present. So that we need to subtract these stresses from the stresses obtained from the stress analysis and upload them as a separate load channel into PragTic. Thus, the loadings are set into PragTic in form of two load channels that are then superimposed: the constant load caused by the bolt pretension and the load cycles that are described in Table 6. The material parameters are implemented into PragTic if form of cyclic curve and strain life curve coefficients. The curves for the temperature 240^oC are chosen. The cyclic curve parameters are taken from relations 5.2 and 5.3 and the strain life curve parameters are taken from relations 5.6, 5.7, 5.8 and 5.9. In Figure 34, the settings of the method can be seen.

Figure 34: SWT method settings in PragTic

5.3.2 The results

The results from PragTic are obtained in form of a text file in which a damage index D is assigned to each node. The damage for each load cycle was also exported, its comparison can be observed in Figure 35 where damage for nodes 1484141, 1492079, 1484055 and 1491993 is plotted.
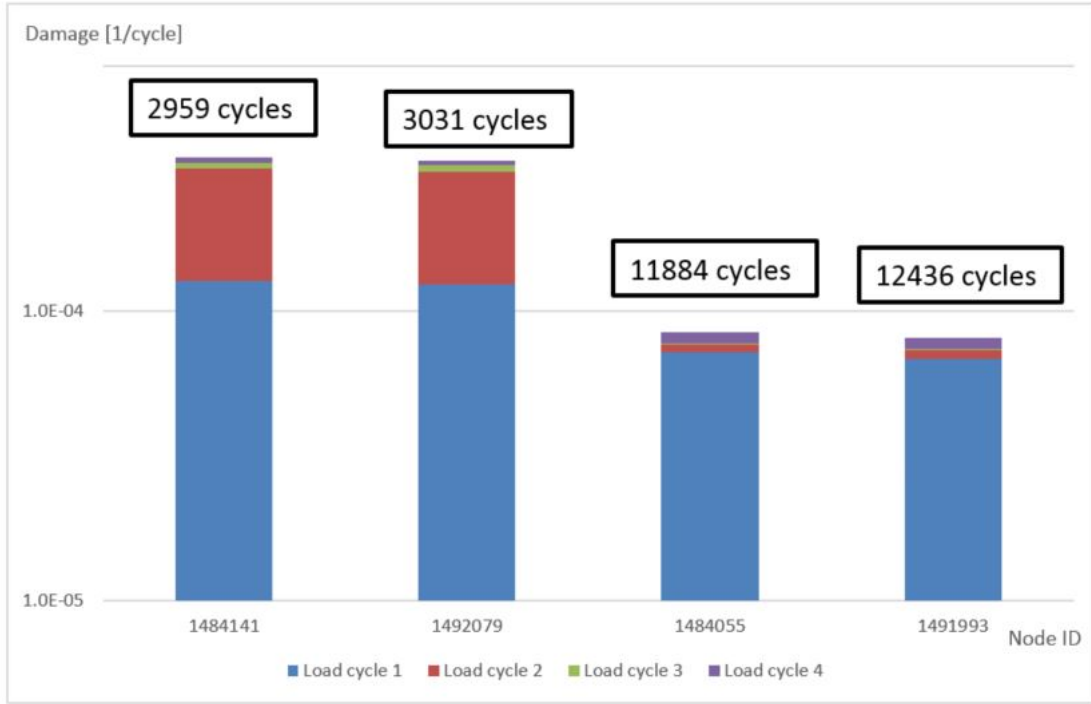
Figure 35: Damage according to SWT method for nodes 1484141, 1492079, 1484055 and 1491993

The first 2 nodes (1484141 and 1492079) have the highest damage according to SWT method. However, we can see in Figure 35 that for these 2 nodes the portion of the damage corresponding to the load cycle 2 is significantly higher compared to the other 2 nodes. This is caused by the influence of the signed von Mises stress. There are several methods how to calculate the sign of the signed von Mises stress and these methods can produce different results. Figure 34 shows that von Mises (signed I1) reduction was used for the calculation. It means that the sign of the von Mises stress is equal to the sign of the first invariant of the stress tensor I_1

$$I_1 = \sigma_1 + \sigma_2 + \sigma_3 \qquad (5.10)$$

Nevertheless, the calculation according to formula 3.25 (SPmax) can be also utilized. This formula uses the sign of the principal stress whose magnitude is the highest. In such case we get different results for stress amplitude and consequently damage caused by the load cycle 2 for nodes 1484141 and 1492079. Table 7 shows maximum and minimum stress tensors in load cycle 2 for nodes 1484141 and 1484055. While in case of node 1484055 signed von Mises stress determined by I1 and SPmax is the same, it differs in case of node 1484141. If we use SPmax method, the sign of the minimum stress in the load cycle 2 is opposite and the stress amplitude is significantly lower. So that we should be careful which method is used.

50

Node ID	Velocity ω [%]	σ_x	σ_y	σ_z	τ_{yz}	τ_{xz}	τ_{xy}	σ_1	σ_2	σ_3	$\sigma_{e,svM}$ (I1)	$\sigma_{e,svM}$(SPmax)
1484141	60	65	23	-88	-5	13	120	166	-70	-96	-250	250
	96	173	63	-161	-11	33	311	435	-145	-214	617	617
										$\sigma_a =$	434	184

Node ID	Velocity ω [%]	σ_x	σ_y	σ_z	τ_{yz}	τ_{xz}	τ_{xy}	σ_1	σ_2	σ_3	$\sigma_{e,svM}$ (I1)	$\sigma_{e,svM}$(SPmax)
1484055	60	88	5	-32	-7	21	117	231	171	-27	231	231
	96	216	6	-110	-18	56	293	592	425	-92	361	361
										$\sigma_a =$	65	65

Table 7: Maximum and minimum stress tensors in load cycle 2 for nodes 1484141 and 1484055

As we want to keep consistency of the method the same signed von Mises reduction (I1) is applied to all the load cycles. However, the results should be handled with caution because of this fact.

In order to see the damage distribution on the whole component, the output file from PragTic is exported to Ansys and the damage is mapped on the impeller. So that we can see the locations with the highest probability of failure. The damage parameter distribution can be seen in Figures 36 and 37.
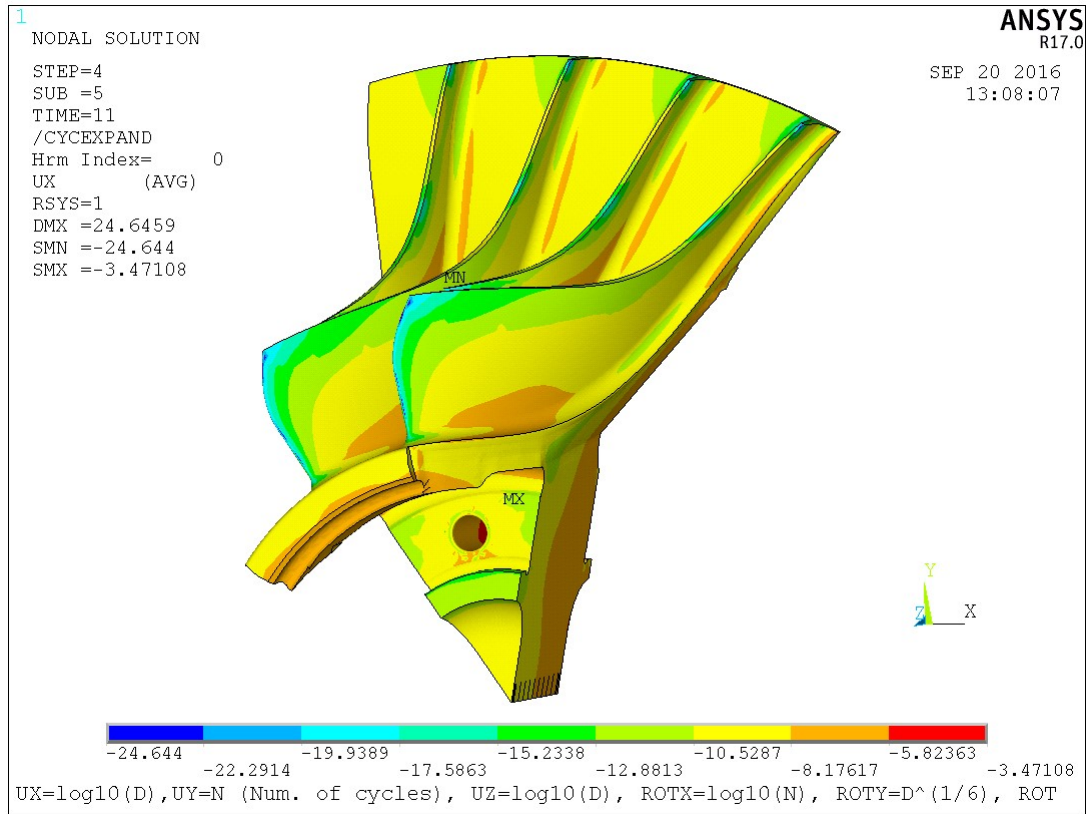
Figure 36: The damage parameter distribution from the front side of the impeller according to the SWT method
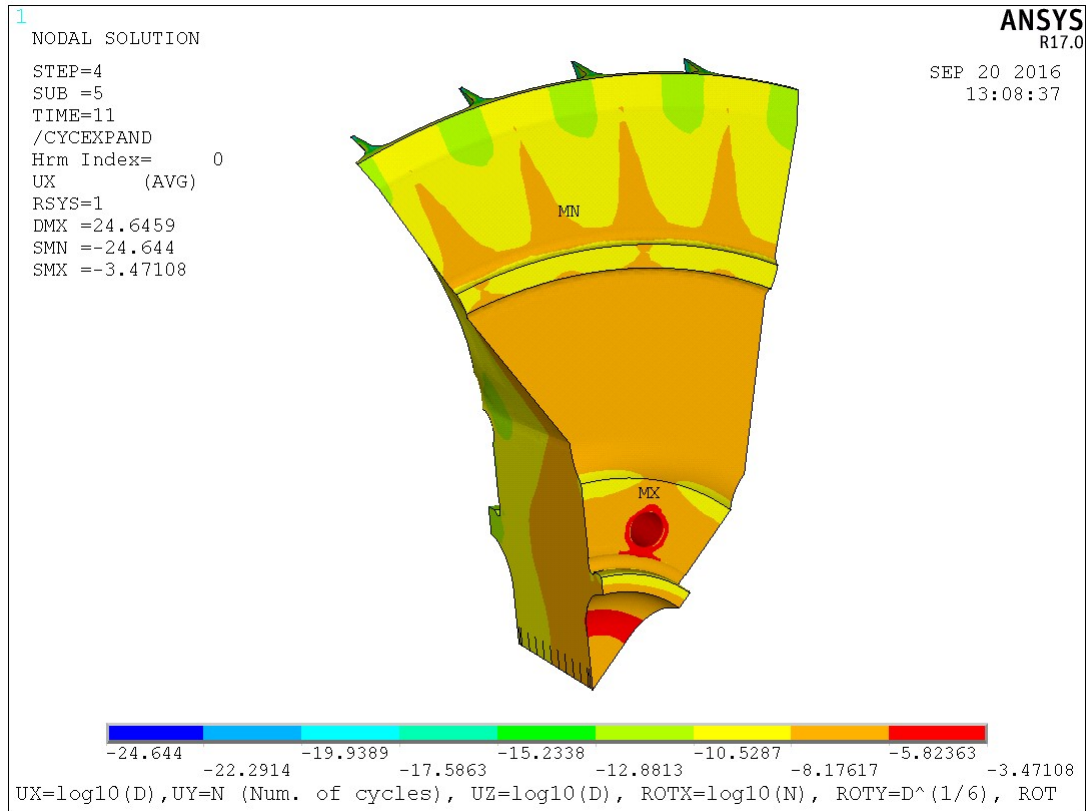
Figure 37: The damage parameter distribution from the back side of the impeller according to the SWT method

For better visualization, a common logarithm of D, $\log(D)$, is plotted in all the figures that show the damage distribution. We can see that the critical location from the fatigue life point of view is again the bolt hole. Figure 38 shows the damage parameter distribution in the bolt hole in more detail and in a different scale so that the critical nodes can be observed.
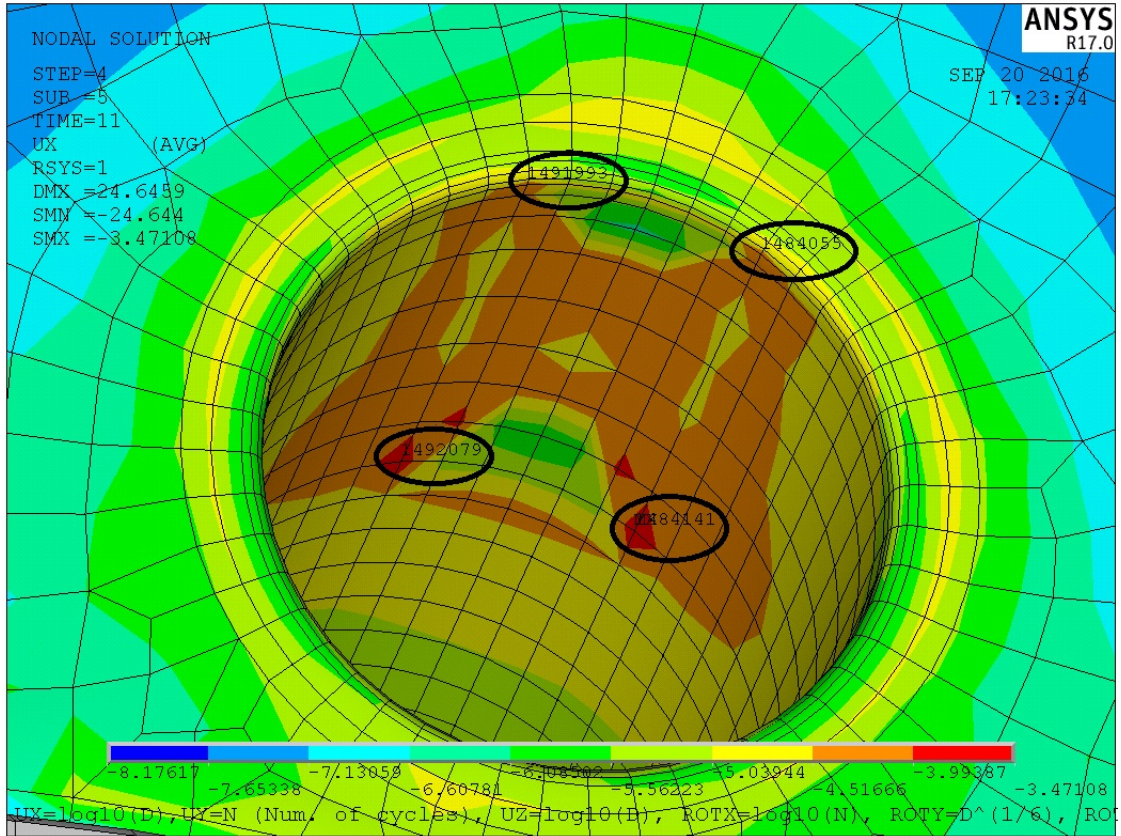
Figure 38: The damage parameter distribution in the bolt hole of the impeller according to the SWT method

The 3 nodes with the highest damage are marked with the black circle. The results from PragTic for these 3 nodes including their ID numbers are summarized in Figure 35. Maximum damage index is 3.38×10^{-4} that corresponds to node number 1484141 and 2959 cycles. Hence, the life of the impeller determined by use of SWT method is 2959 equivalent cycles.

5.4 Fatigue assessment using Landgraf method

5.4.1 The input data implementation

Fatigue assessment using Landgraf method is also performed in the PragTic software. The loading history, material parameters, the method settings and FEA results are the same as in case of the SWT method. The only difference is in an assumption how the means stress affects the final solution.

5.4.2 The results

The results from Pragtic can be observed in Figure 39. The bolt hole is again the most critical location.
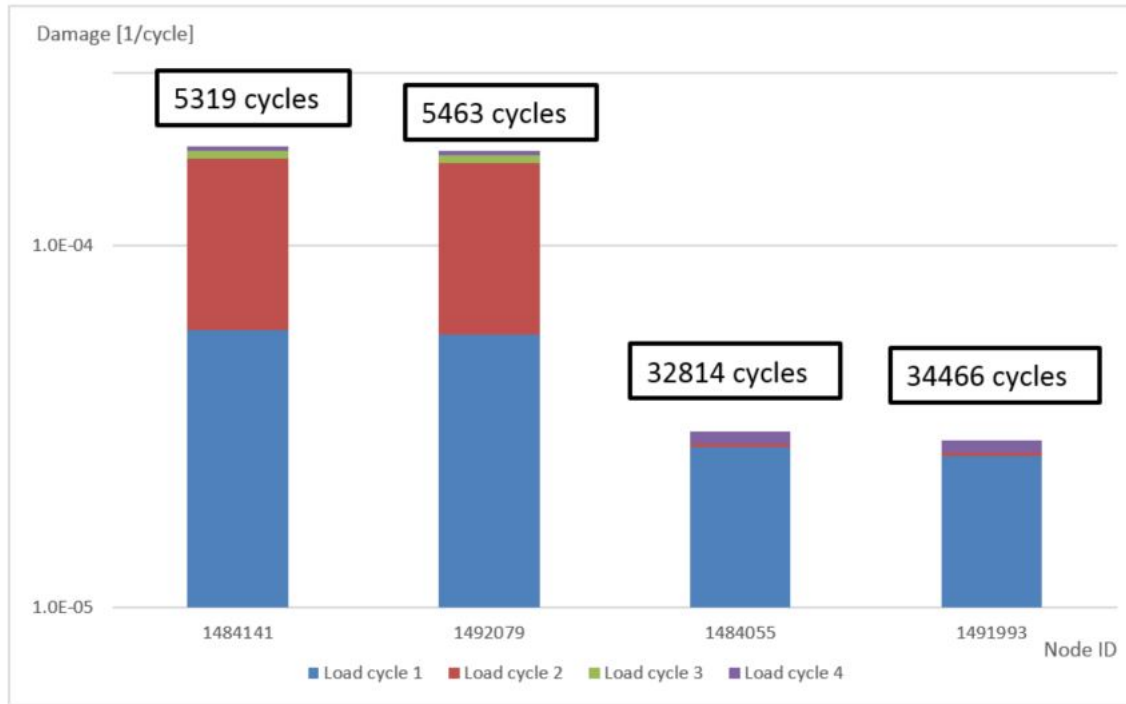
Figure 39: Damage according to Landgraf method for nodes 1484141, 1492079, 1484055 and 1491993

The highest damage is again in node number 1484141. It is 1.88×10^{-4} which corresponds to 5319 cycles to crack initiation. The damage parameter distribution can be seen in Figures 40 and 41.
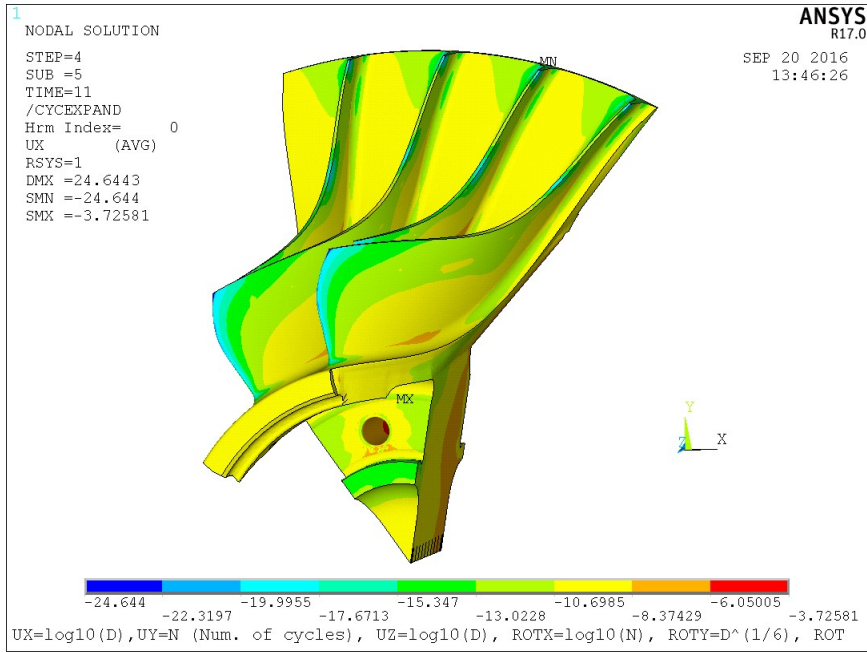
Figure 40: The damage parameter distribution from the front side of the impeller according to the Landgraf method

Figure 41: The damage parameter distribution from the back side of the impeller according to the Landgraf method

5.5   Fatigue assessment using historical GEAC method

Based on the results from PragTic software, we consider nodes with numbers 1484141, 1492079 and 1484055 as the most critical ones in terms of the fatigue life. Therefore, the historical GEAC method is employed to determine the fatigue life only for these nodes. Stress tensors in these nodes obtained from the FEM analysis are shown in Table 8. They are selected 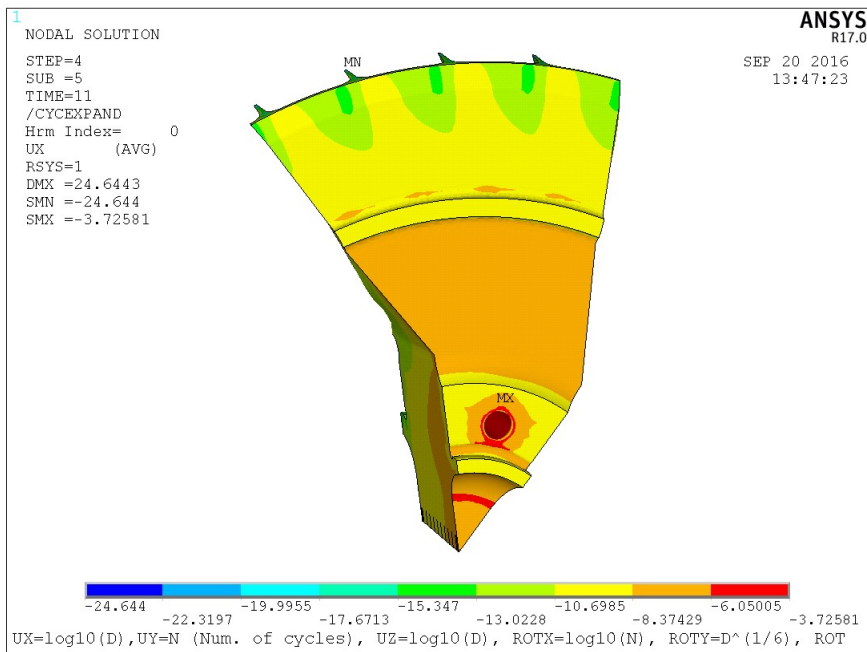for rotational velocity 0% and 100% as having these two tensors we are able to calculate stress tensor for any other rotational velocity since the FEM analysis is linear.

Rotational velocity ω [%]	Temperature [°C]	σ_x [MPa]	σ_y [MPa]	σ_z [MPa]	τ_{xy} [MPa]	τ_{yz} [MPa]	τ_{xz} [MPa]	σ_{ekv}^{SGN} [MPa]
Node 1484141								
0	23	-5.03	-2.24	-41.38	-2.88	-1.07	0.21	- 38.20
100	238	188.79	68.25	-171.28	337.96	-11.83	35.865	669.11
Node 1492079								
0	23	-6.5788	-0.48863	-41.312	0.65546	-1.0677	0.39603	-38.21
100	235	427.98	-172.97	-171.85	-162.65	-25.632	-29.607	666.66
Node 1484055								
0	23	-1.53	-0.29	-22.26	-0.60	0.06	0.20	15.06
100	235	234.02	5.9218	-121.23	318.29	-19.746	60.978	643.00

Table 8: FEA stress results for the selected nodes 1484141, 1492079 and 1484055

Due to the multiaxial stress state of the structure, we use Manson-McKnight method for reduction to the uniaxial stress state. The results below are for the sake of simplicity presented only for the most critical node 1484141. The elastic equivalent mean stress and amplitude according to this method for the most critical node 1484141 are:

$$\sigma_{m,FE} = 341.2 MPa \tag{5.11}$$

$$\sigma_{a,FE} = 328.9 MPa \tag{5.12}$$

These stresses are calculated for load cycle that starts when the engine is subjected to 0% of nominal speed, then is accelerated to 100% of nominal speed and then decelerated back to 0%. From these two values, maximum and minimum stress of this cycle are:

$$\sigma_{max,FE} = 670.1 \ MPa \tag{5.13}$$

$$\sigma_{min,FE} = 12.2 \ MPa \tag{5.14}$$

However, we do not have only one load cycle. It is needed to consider all the load cycles in the load history of the component (see Table 6). If the stresses

induced by temperature in the structure are neglected, the resulting stress state can be considered as proportional to the centrifugal force caused by the rotational velocity. Hence, we determine the uniaxial stress σ at the certain rotational velocity ω according to the following formula since the centrifugal force is proportional to ω^2:

$$\sigma = \frac{(\sigma_{max,FE} - \sigma_{min,FE})\omega^2}{100^2} + \sigma_{min,FE} \tag{5.15}$$

Using this formula, we are able to obtain the uniaxial maximum and minimum stresses for all the load cycles. For the cycle 1 in the loading history(from 0% to 100.4% of the nominal speed), the maximum and minimum uniaxial stresses are:

$$\sigma_{max,FE} = 675.4 \ MPa \tag{5.16}$$

$$\sigma_{min,FE} = 12.2 \ MPa \tag{5.17}$$

However, this should be handled with caution because the stresses determined by 5.15 are elastic stresses. In order to determine the real stress state we need to use elastic-plastic correction. This is carried out according to Figure 42, where we can see the correction for the maximum stress in the load cycle 1..
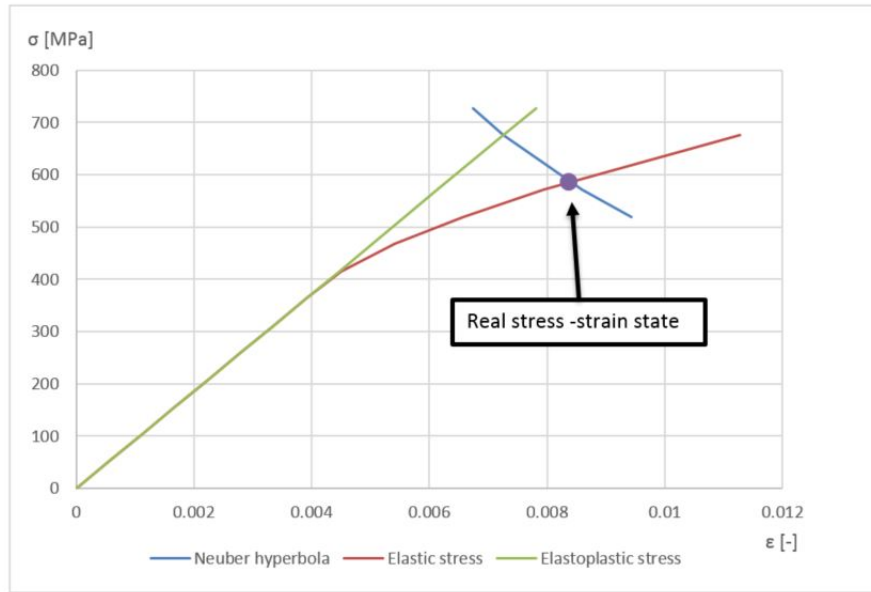

Figure 42: Neuber correction of the maximum stress in node 1484141

The maximum real stress in the first cycle, σ_{real}, is then determined from the Neuber hyperbola that is given by equation:

$$\frac{(\sigma_{max,FE})^2}{E} = \sigma_{real}\epsilon_{real} \tag{5.18}$$

58

where $\sigma_{max,FE}$ is determined from equation 5.16 and ϵ_{real} is obtained from the Ramberg-Osgood curve as:

$$\epsilon_{real} = \frac{\sigma_{real}}{E} + \left(\frac{\sigma_{real}}{K}\right)^{\frac{1}{n}} \tag{5.19}$$

By combination of relations 5.18 and 5.19,the maximum real stress is reduced to:

$$\sigma_{real} = 585.8 \ MPa \tag{5.20}$$

Next, we need to find the real stress and strain amplitudes for the load cycle 1. The Neuber correction is used again but now it is for the cyclic loading. The neuber hyperbola is defined by:

$$\frac{\Delta\sigma_{elastic}}{E_{cyc}} = \Delta\sigma_{real}\Delta\epsilon_{real} \tag{5.21}$$

where

$$\Delta\epsilon_{real} = \frac{\Delta\sigma_{real}}{E_{cyc}} + 2\left(\frac{\Delta\sigma_{real}}{2K'}\right)^{\frac{1}{n'}} \tag{5.22}$$

Using relations 5.21 and 5.22, the stress and strain amplitudes are:

$$\epsilon_a = 6.5 \times 10^{-3} \tag{5.23}$$
$$\sigma_a = 329.0 \ MPa \tag{5.24}$$

Eventually we need to determine a mean stress of the first load cycle, σ_m, that is according to 3.15:

$$\sigma_m = 256.8 \ MPa \tag{5.25}$$

The Neuber parameter for the first load cycle is then:

$$\sigma_{Neuber} = 442.4 \ MPa \tag{5.26}$$

The Neuber parameter is then used for a determination of maximum number of cycles for maximum and minimum temperature during the cycle. The lower number is considered as the final result. The same procedure is used for all the cycles from Table 6. The damage from each load cycle for all the investigated node can be seen in Figure 43.
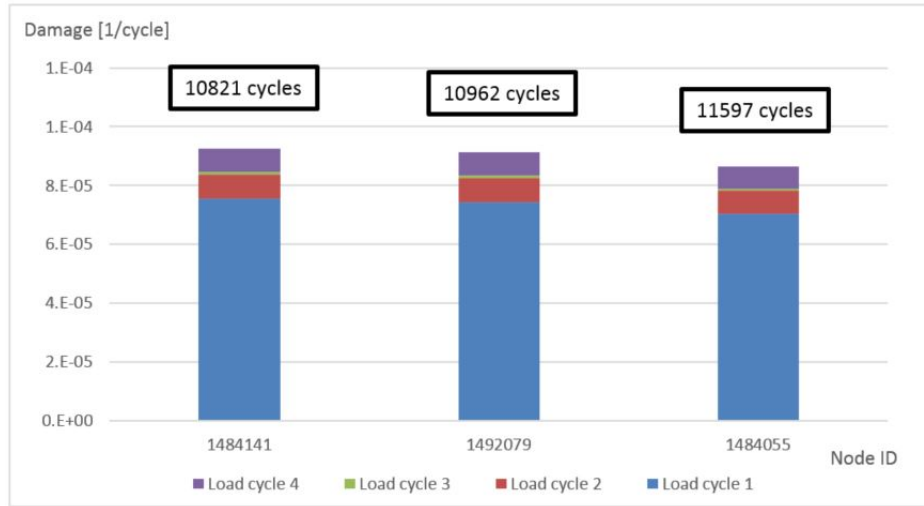
Figure 43: Damage distribution for nodes 1484141, 1492079 and 1484055 determined by historical GEAC method

The final results for all nodes from Table 8 are in the Table below:

Node No.	N for T_{max}	N for T_{min}	Total N
1484141	10821	30603	10821
1492079	10963	31002	10963
1484055	11579	41002	11579

Table 9: Fatigue life for nodes 1484141, 1492079 and 1484055

5.6 Fatigue assessment using the method proposed by Nagode

5.6.1 The input data implementation

The input data required for this method are: load history and material parameters for several temperatures. The load history is implemented into the calculation as a sequence of signed von Mises stresses that the component repeatedly experience. For this reason, the load history defined in Table 6 is simplified in this case. Only the first two cycles are considered as it would be complicated to implement the cycle 3 a 4 because their occurrence per equivalent cycle is much lower than 1. The load history for the critical node 1484141 is depicted in Figure 44 where the stresses are corrected by Neuber formula(3.8).
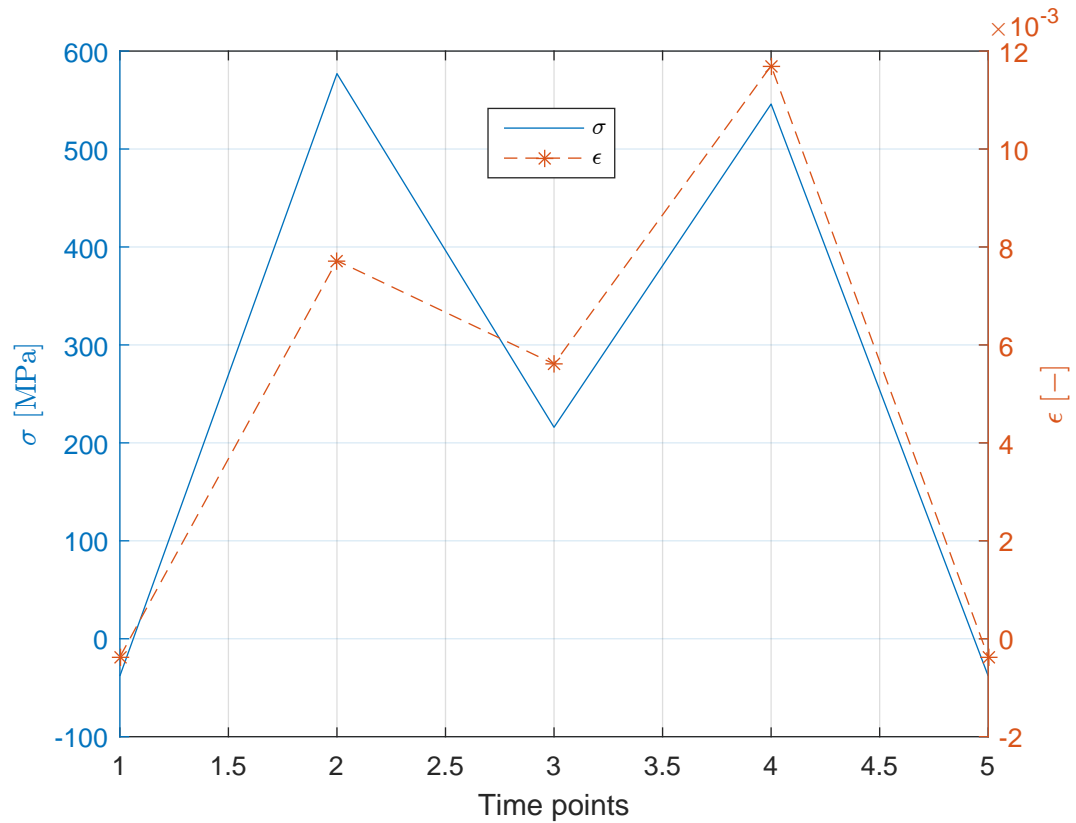
Figure 44: The load history for node 1484141

The corresponding strain response to the load history is also shown in Figure 44. It was calculated only in the turning points by using 3.9. Stress and strain history is summarized in Table 10.

Time point	1	2	3	4	5
Stress [MPa]	-38	577	216	545	-38
Strain [-]	-3.71E-04	7.72E-03	5.61E-03	1.17E-02	-3.71E-04

Table 10: Stress and strain history for node 1484141

For this method, we need a strain-life curve for each temperature that is in the load history. Since only strain-life for 3 temperatures are available, the remaining curves for the other temperatures from the load history are piecewise cubic Hermite interpolated.

The LCF calculation is performed by use of a set of functions in a c++ library that was developed in CTU. The input data were read in a form of text files and compiled through the Windows command line.

5.6.2 The results

In Figure 45, we can see how the SWT parameter, σ_{SWT}, is changing with time according to Nagode's method.
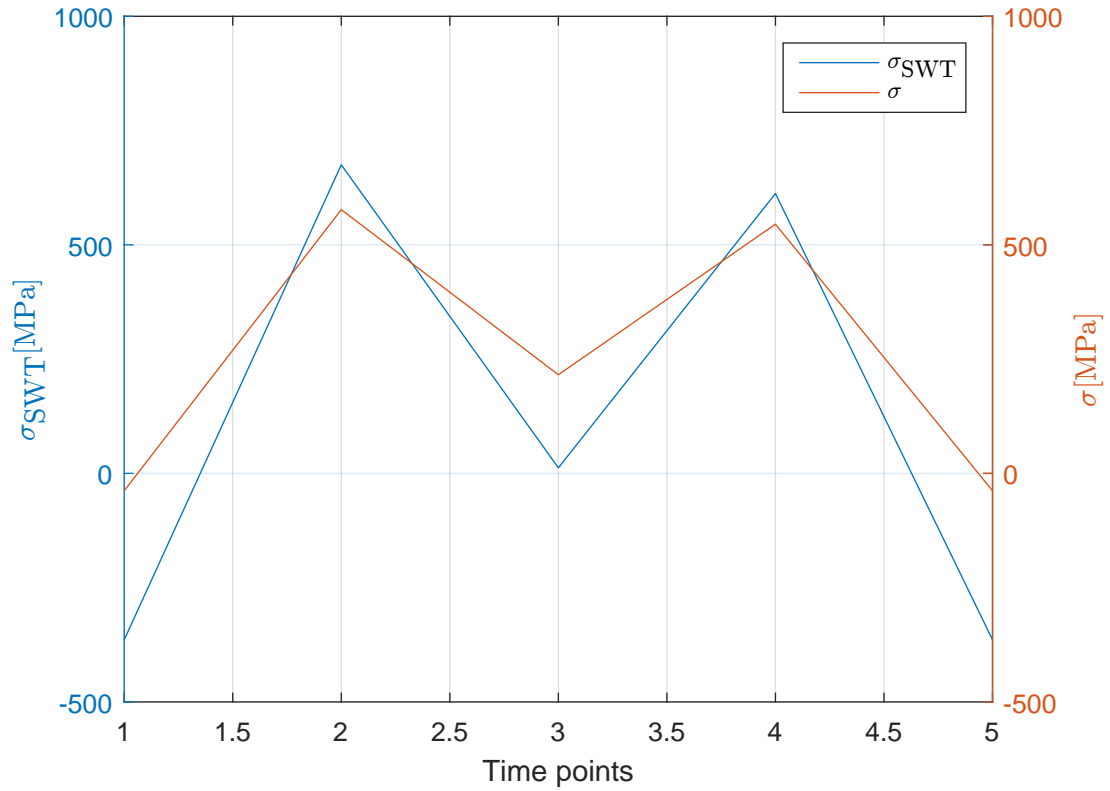

Figure 45: σ_{SWT} and σ vs time for node 1484141

Figure 46 shows how the damage D develops with time when the load history is applied.
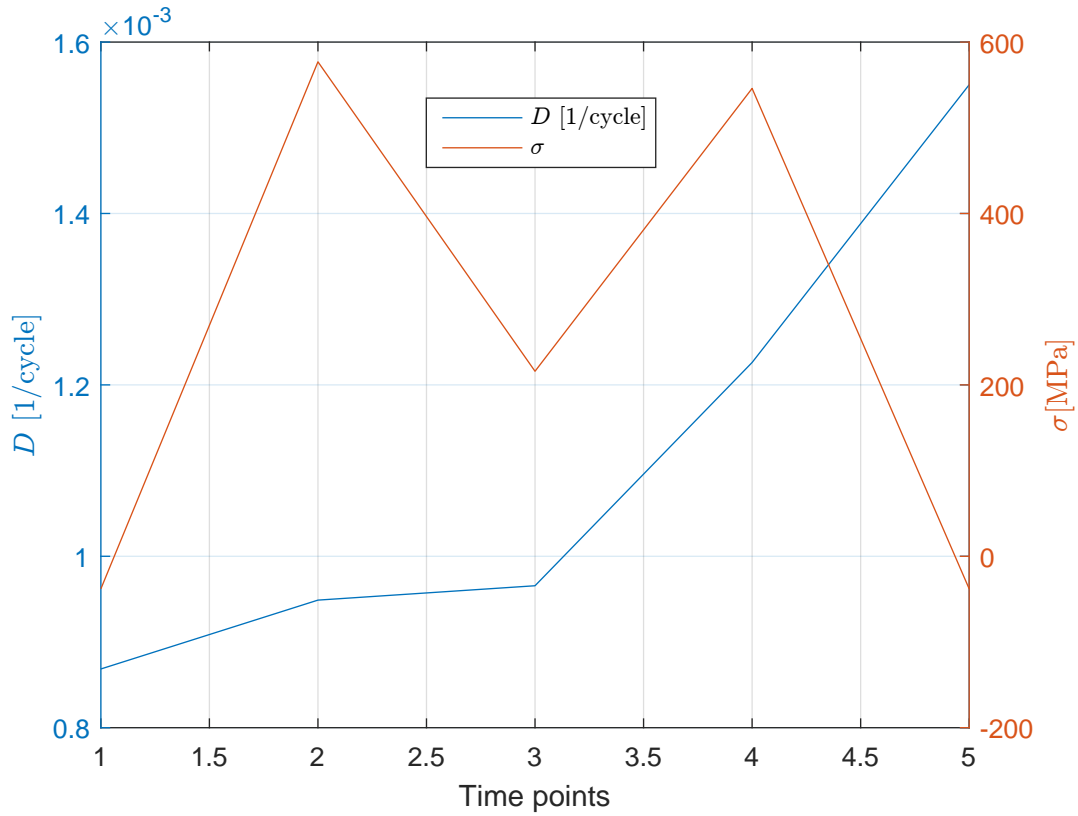
Figure 46: Damage D and σ vs time for node 1484141

The total damage according to the formula 3.37 is

$$D_{accum} = 0.000681704 \text{ cycle}^{-1} \tag{5.27}$$

It corresponds to 1467 equivalent cycles until crack initiation appears.

5.7   Fatigue life results comparison

The results from the LCF methods are compared at 2 critical nodes 1484141 and 1484055. Table 11 shows the comparison of the SWT method, Landgraf method and the historical GEAC method. The critical node in terms of fatigue is node 1484141 for all the methods. The highest life is estimated by the historical GEAC method while SWT method predicts the lowest life. As discussed before, the main reason for that is the different method of the signed von Mises stress calculation. On the other hand, the estimated life from the SWT and historical GEAC method for node 1484055 is comparable. This is caused by the fact that the signed von Mises stress is the same for both methods during the whole load history in this node. Besides, the fatigue life obtained from the Landgraf method is generally higher than the fatigue

Node ID	SWT method	Landgraf Method	GEAC method
1484141	2959	5319	10821
1484055	11884	32814	11579

Table 11: The results comparison for the SWT, Landgraf and historical GEAC method

life obtained from the SWT method. This is caused by the different way of mean stress inclusion into the calculation.

The method proposed by Nagode was applied only to the most critical node 1484141. The result is the most conservative as the fatigue life determined by Nagode's method is only 1467 cycles.

6 Conclusion

The impeller alternative design of the H80 engine has been analysed. The thermal and structural analysis was performed using FEM software Ansys 17. The FEM analysis was done for the acceleration to the maximum speed and the consequent deceleration. This mission was divided into 10 time steps. Each time step is characterized by different velocity, temperature and aero gas loads therefore in each time step the corresponding loads were applied. From the FEA results, we could see that the temperature influence on the stress state of the impeller is negligible as the increase in von Mises stress in the critical node was within 3% during the acceleration to the maximum speed.

Modal analysis was performed for:

- the unloaded impeller

- only mechanically loaded impeller

- thermally and mechanically loaded impeller

Seven natural frequencies and corresponding modes shapes have been obtained. Natural frequencies were the lowest in case of the unloaded impeller. It corresponds to the assumptions since the unloaded component has the lowest stiffness. However, these frequencies are similar to the eigenfrequencies of the thermally and mechanically loaded impeller since temperature decreases the stiffness of the component.

Based on the FEM analysis, the fatigue life calculation has been carried out. Four different methods were used to evaluate the low cycle fatigue of the impeller and the results were presented. The calculation was performed in software developed at Czech Technical University. The critical location in terms of fatigue is in the bolt hole of the impeller. The most conservative result 1467 cycles is predicted by the method proposed by Nagode. This method takes into account the temperature change in every time point of the mission. On the other hand, the highest life 10821 cycles was determined by the historical GEAC method.

This analysis is a demonstrative case conducted to compare different lifing methods, therefore results will not be used for real purposes.

References

[1] Rosa, U.; Nagode, M.; Fajdiga, M. *Strain-life approach in thermo-mechanical fatigue evaluation of complex structures.* Fatigue & Fracture of Engineering Materials & Structures Vol. 30, No. 9, 2007, pp. 808-822.

[2] Hack, M.; Nagode, M.; Fajdiga, M. *Low cycle thermo-mechanical fatigue: damage operator approach.* Fatigue & Fracture of Engineering Materials & Structures

[3] Papuga, J. *Help for PragTic v.0.2betaH.* Brtnice 2007.

[4] ANSYS. *ANSYS User's Manual.* Version 16.

[5] Bishop, N.W.M.; Sherrat, F. *Finite element based fatigue calculations.* NAFEMS Ltd., 200016.

[6] Brokate, M. and Sprekels, J. *Hysteresis and phase transitions.* Applied Mathematical Sciences, 121.Springer Verlag, New York, USA

[7] Růžička, M.; Hanke,M.; Rost, M. *Dynamická pevnost a životnost.* Skripta ČVUT v Praze, 1992, Vyd. 2. přeprac.

[8] Nihei, M.; Heuler, P.; Boller, C. *Evaluation of mean stress effect on fatigue life by use of damage parameters.* International Journal of Fatigue Vol. 8., No. 3, 1986, pp 119-126

[9] Norberg, S.; Olsson, M. *The effect of loaded volume and stress gradient on the fatigue limit.* International Journal of Fatigue Vol. 29., No. 12, 2009, pp 2259-2272

[10] POLÁK, J. *Cyklická plasticita a nízkocyklová únavová odolnost kovových materiálů.* Praha : Academia, 1986

[11] Bolotin, V. V *Mechanics of fatigue materiálů.* Mechanical engineering series, 1999

[12] Liu, G.R. and Quek, S.S. *The Finite Element Method: A Practical Course.* Butterworth-Heinman, Oxford, 2003